Evaluation of Alternative Direction of Arrival Methods for Oceanographic HF Radars

Brian Emery, *Member, IEEE,*

Abstract

The majority of ocean current measuring HF radars obtain the direction of arrival (DOA) of signals backscattered from the ocean with the Multiple Signal Classification (MUSIC) algorithm. These radars often operate under conditions including low SNR, low numbers of data samples (aka snapshots), and with the number of signal sources approaching or exceeding the number of receive antenna elements. Improving the accuracy and coverage of the radar data in these situations would improve data produced by radar networks such as the U.S. Integrated Ocean Observing System (U.S. IOOS), revealing new understanding of coastal ocean dynamics. This paper presents an evaluation of DOA techniques developed over the last 10-20 years, for application to oceanographic HF radars using a simulation based approach. Simulations performed using three commonly used receive arrays suggest that the use of Maximum Likelihood Estimation by Alternating Projection (MLE-AP, [1]) leads to similar accuracy, with improvement in coverage due to the higher number of DOA solutions obtained when compared to MUSIC. These advances come at a higher computational cost, though the difference is manageable. The analysis also illustrates the need to identify and evaluate signal detection methods (i.e. methods to identify the number of simultaneous souce bearings) to work in conjunction with MLE-AP. Overall, these results suggest improvements in the data coverage of ocean current maps produced by HF radars, and thus in the many practical applications employing them such as spill response, and search and rescue.

Keywords

Direction finding, current measurement, HF radar, ocean current, radio oceanography, simulation

---

B. Emery is with the Marine Science Institute, University of California, Santa Barbara, CA, 93106 USA e-mail:brian.emery@ucsb.edu.

Manuscript in preparation, draft 2018

Evaluation of Alternative Direction of Arrival Methods for Oceanographic HF Radars

I. Introduction

Drivers of coastal ocean currents such as wind stress, pressure gradients, and buoyancy forcing interact with the coastal boundary resulting in highly variable and spatially complex flows. Observations that capture these flows in space and time are used to quantify the surface transport of particles or pollutants in spill responses and search and rescue operations [2]. Land based HF radar is the only cost effective observational approach capable of resolving the temporal and spatial scales needed to understand the dynamics of coastal circulation.

Despite their success in many applications, HF radars are limited in their ability to observe complex, small scale flows. For example, a radar installation with 400 m resolution [3], [4], found substantial contribution to the total exchange across the shelf from highly complex eddies with spatial scales ~ 1 km and mean durations of ~ 5 hours. A more in depth analysis of the eddy dynamics was hampered by the errors of the radar system, which increased by a factor of two in areas of increased flow complexity [5]. Furthermore, a high resolution numerical model of the Santa Barbara Channel [6], [7] reveals flow structures not found in HF radar observations (e.g. Fig. 1). While HF radar observations are often usefully combined other observational approaches and models in coastal oceanographic studies (e.g. [8], [9]), investigations to reduce inherent error in the measurements are warranted [10]–[12].

The development of the oceanographic HF radar coincided with the invention of the Multiple Signal Classification (MUSIC) algorithm for direction of arrival (DOA) processing [13]–[16]. The use of MUSIC by the SeaSonde, the commercial product developed by CODAR Ocean Sensors, Ltd., followed the earlier Coastal Ocean Dynamics Application Radar (CODAR), which used a least squares approach to DOA processing [17]. The computational efficiency of MUSIC enabled the use of low cost personal computers, which when combined with a spatially compact receive array, likely contributed to the fact that the SeaSonde constitutes the majority of deployed systems. With a few exceptions (e.g. [18]–[22]), application of MUSIC in oceanographic contexts has been specific to the SeaSonde, which until recently was protected by U.S. Patent [23]. In

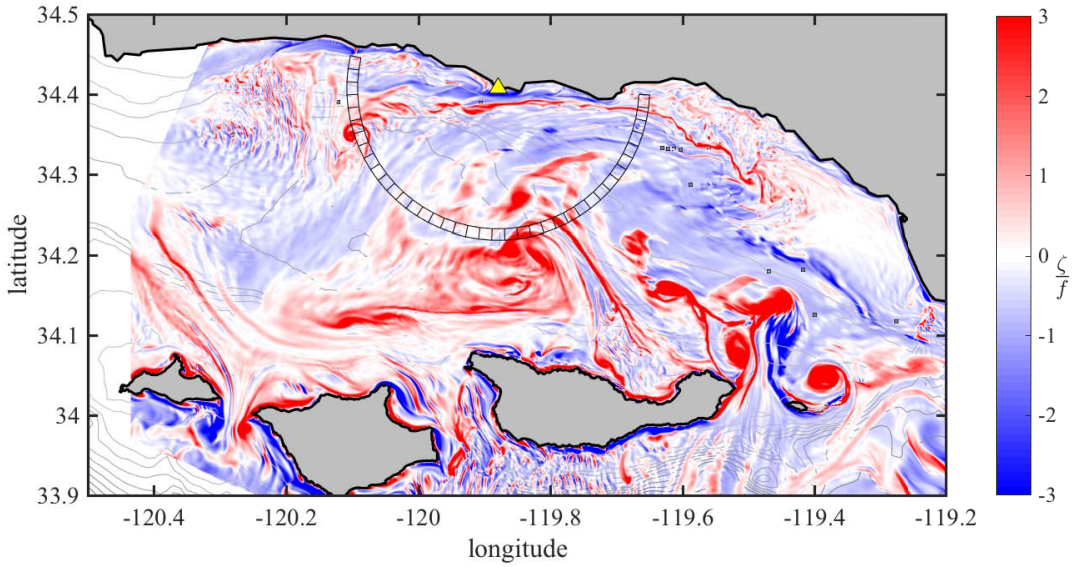

Fig. 1. Vorticity (ζ) normalized by planetary vorticity (f) from 100 m resolution ROMS [6], [7], showing the location of the simulated HF radar (yellow triangle), and a 1.5 km wide range cell at 19.5 km, with 5^o increments.

the decades since the publication of MUSIC and its application to oceanographic radars, many alternative methods for DOA processing have been developed outside of the oceanographic community, each claiming some advantage over MUSIC.

In this study the most promising algorithms for improving extractions of radar-based ocean current data are described and evaluated in the specific context of ocean current measuring radars. While the literature on direction finding methods suggests certain advantages and disadvantages for the various DOA methods (e.g. [1], [24], [25]), identifying an advantage for a particular method requires a comparative evaluation in the specific application as defined by, for example, the number of simultaneous signal source, typical SNRs, and antenna geometries, etc. [25].

The goals of this study are to evaluate alternative direction finding methods, seeking an improved ability to resolve complex coastal flow structures. To evaluate the performance of DOA algorithms, the analysis employs a simulation based approach (e.g. [26]–[29]), with the difference of using complex flows from the high resolution Regional Ocean Modelling System (ROMS; [6], [7]) as the simulation inputs (Fig. 1). Simulations allow the direct evaluation of algorithm performance in scenarios closely resembling the planned application, without the confounding

factors associated with in situ comparison (e.g. [30]–[32]). The use of ROMS as the input current field represents a robust, and perhaps realistic test of DOA methods as applied by oceanographic radars.

The paper is organized as follows. Section II reviews signal processing methods for oceanographic HF radars. Section III defines the two signal models used for simulating signals received by the HF radar. DOA methods used in the study are described in Section IV, some experimental details are reviewed in Section VI, and the results and conclusions are presented in Sections VII, and VIII respectively.

II. HF Radar Techniques

Prior to discussing the models used to simulate HF radar backscatter, and the DOA methods investigated, the relevant signal processing used by oceanographic HF radars are reviewed. This review generally follows previous discussions specific to the SeaSonde ([12], [23], [28], [33]), but the methods can be applied to radar systems with arbitrary antenna configurations.

A typical HF radar transmits a frequency modulated signal (near 5, 13, or 24 MHz) that couples with the sea surface in ground wave propagation. The signals backscatter from Bragg resonant ocean surface waves [34], [35] with a wavelength $\lambda = \frac{\lambda_{TX}}{2}$, where λ_{TX} is the wavelength of the transmitted radio wave. The ocean surface waves impart a Doppler shift due to the combination of their phase speed and that of the radial component of the underlying ocean surface current ($\mathbf{v}_r$). The effective depth of $\mathbf{v}_r$ is a function of the wavelength of the resonant ocean wave (and thus the transmit frequency), and ranges from 2.5-0.5 m for 5-24 MHz radars [36], [37]. Demodulation sorts the received signals as a function of range r, with the range increment (δr) determined by the transmit bandwidth (BW) [38],

$$\delta r = \frac{c}{2BW}, \tag{1}$$

given the speed of light $c = 3\times10^5$ km s^{-1}. Windowing in the FFT processing of the demodulated signal produces 15% overlap between range cells for SeaSondes, and up to 50% for other systems (e.g Wellen Radars (WERA)) [39]. For a given range, observations from sequential transmit sweeps produce a time series (c.f. [23]), which forms the input to Doppler resolving FFTs. Taking the conjugate products [40] of the Doppler FFTs then forms the auto- and cross-spectra. The resulting spectra sort the signal variance by frequency, revealing peaks near frequencies

$f_B = \pm\sqrt{\frac{g}{\pi\lambda_{TX}}}$, where g is the acceleration of gravity, corresponding to the theoretical speed of the approaching and receding Bragg resonant ocean waves [34]. Spread in the of the energy content in the Bragg peaks around f_B results from variation in the underlying radial currents $\mathbf{v}_r$.

A typical SeaSonde produces estimates of the Doppler spectra every 256 s, using a 2 Hz sweep rate (SWR) such that $n_{FFT} = 512$. The SeaSonde outputs averaged spectra every 10 minutes, combining 3 FFTs which cover a total of 12 min and 48 s. The FFT length sets the frequency bin width, $\delta f = \frac{SWR}{n_{FFT}}$, and from δf the resolution of $\mathbf{v}_r$ is computed,

$$\delta\mathbf{v}_r = \frac{\lambda_{TX}\delta f}{2}. \tag{2}$$

For a 13 MHz radar with $n_{FFT} = 512$, $\delta\mathbf{v}_r \approx 4$ cm s^{-1}. Longer FFT lengths improve bin resolution (to e.g. $\sim 1-2$ cm s^{-1} [3], [39]), particularly when combined with a higher SWR (e.g. $SWR \approx 3-4$ Hz [41]).

Doppler power spectra typically resolve a main peak, centered on f_B for example, containing signal from the first order resonant backscatter, with lower peaks at adjacent frequencies resulting from higher order scattering processes [35]. Only signal from the first order scatter contains ocean current information for DOA processing. SeaSondes use empirical methods [33] to identify the first order region, though image processing techniques have recently been adapted for the purpose [42].

For each f in the first order region the $M \times M$ covariance matrix $\mathbf{C}(f)$ is formed (e.g. [33], [40]) from bin values of the averaged auto- and cross-spectra, where M is the number of receive antennas. Studies in the signal processing literature typically apply DOA processing to covariance matrices formed directly from the antenna voltage time series [43], [44], rather than to $\mathbf{C}(f)$ from the frequency domain. The FFT pre-processing described here sorts variance by Doppler frequency, and hence velocity, allowing application of DOA processing to individual Doppler velocities. The consideration of individual narrow ranges of frequency, increases the likelihood that the signal emanates from a small fraction (or a few separate, small fractions) of the total azimuthal range. This step, referred to as narrowband processing [25], decreases the number of simultaneous source bearings.

Determining the number of simultaneous DOAs present in $\mathbf{C}(f)$ constitutes the next step in the processing scheme. The SeaSonde uses a hypothesis testing approach [33] to determine if the data in $\mathbf{C}(f)$ results from one or two bearings. Other methods solving the general problem of

determination of the number of simultaneous signal sources exist (known as signal detection e.g. [45]) but will not be addressed here. This study uses the known current input field to determine the number of source DOAs, described in Section VI.

DOA processing associates $\mathbf{v}_r$ with a direction (θ), producing a polar map of $\mathbf{v}_r = \mathbf{v}_r(r, \theta, t)$ for the time (t) and range (r) represented by $\mathbf{C}(f)$. SeaSondes commonly produce these maps at 10-minute intervals, merging together seven maps at hourly intervals and outputting the median (by default) [46]. Further processing steps not discussed here combine radial maps from several HF radars to produce the total vector surface current estimates using least squares [17], optimal interpolation [47], [48], or other techniques [49], [50]. This analysis focuses on the production of $\mathbf{v}_r(r, \theta, t)$, since these form the basic data product of individual HF radars.

III. Simulation Signal Models

A. General Array Data Model

The simulation of signal backscattered from the ocean surface can be considered a special case of a more general array data model (e.g. [16], [44], [51]). The general model describes the voltages received ($\mathbf{Y}$) on each of the M antennas as a function of the array response $\mathbf{A}$, the signal sources $\mathbf{X}(t)$, and the noise $\mathbf{e}(t)$,

$$\mathbf{Y} = \mathbf{A}\mathbf{X}(t) + \mathbf{e}(t). \tag{3}$$

The $M \times N$ matrix $\mathbf{A}$ gives the typically complex valued response of the M antennas to the N signal sources located at $\theta_1, \theta_2, ..., \theta_N$ as a function of the antenna pattern at those angles $\mathbf{a}(\theta_1), \mathbf{a}(\theta_2), ..., \mathbf{a}(\theta_N)$ such that,

$$\mathbf{A} = \begin{bmatrix} | & | & & | \\ \mathbf{a}(\theta_1) & \mathbf{a}(\theta_2) & ... & \mathbf{a}(\theta_N) \\ | & | & & | \end{bmatrix}. \tag{4}$$

The $N \times K$ matrix $\mathbf{X}(t)$, where K is the number of independent data samples, or 'snapshots' [43], represents signal from the N sources. After computing the $M \times K$ matrix $\mathbf{Y}$ with (3), the $M \times M$ covariance matrix is computed,

$$\mathbf{C} = \frac{1}{K}\mathbf{Y}\mathbf{Y}^H, \tag{5}$$

where H denotes the Hermitian conjugate.

The analysis uses two implementations of the signal model (as described in [12]), the first with a relatively simple $\mathbf{X}(t)$, and the second with $\mathbf{X}(t)$ designed to model backscatter from the ocean surface.

B. Discrete Source Model

The first implementation of the signal model defines $\mathbf{X}(t)$ for up to $M-1$ point sources as an $N \times K$ collection of zero mean, normally distributed random numbers X_t, with each time step $t = 1, 2, ..., K$ independent [43],

$$\mathbf{X}(t) = \begin{bmatrix} x_1(t_1) & x_1(t_2) & \cdots & x_1(t_K) \\ \vdots & \ddots & & \vdots \\ x_N(t_1) & x_N(t_2) & \cdots & x_N(t_K) \end{bmatrix}. \tag{6}$$

Radar simulations with this model remove much of the complexity present in oceanographic HF radar data, while retaining fundamental performance differences depending only on the receive antenna and the DOA method. Identifying the differences informs the analysis of more complex simulations.

C. Oceanographic Source Model

The second implementation of the signal model simulates signal received by oceanographic HF radars by using (3) with $\mathbf{X}(t)$ defined:

$$\mathbf{X}(t) = \boldsymbol{\gamma}_+ \exp\left(i(\omega_B + \boldsymbol{\omega}_c)t\right) + \boldsymbol{\gamma}_- \exp\left(i(-\omega_B + \boldsymbol{\omega}_c)t\right), \tag{7}$$

where $\boldsymbol{\gamma}_\pm$ is a decorrelation factor (discussed below), $\pm\omega_B$ is the frequency shift due to advancing and receding Bragg waves, and $\boldsymbol{\omega}_c$ is the frequency shift resulting from the ocean currents. In (7), $\exp\left(i(\pm\omega_B + \boldsymbol{\omega}_c)t\right)$ models the total frequency shift due to the combined effects of the Bragg waves and the currents. Here $\omega_B = (2k_{TX}g)^{\frac{1}{2}}$ is a function of the radar wave number $k_{TX} = \frac{2\pi f_{TX}}{c}$, while $\boldsymbol{\omega}_c = 2k_{TX}\mathbf{v_r}$ is a function of the radial velocity of input ocean current field ($\mathbf{v}_r$). The dependence of $\mathbf{v_r}$ on θ causes $\boldsymbol{\omega}_c$ to also depend on θ. Thus the dependence of (7) on $\mathbf{v}_r$ defines $X(t)$ at all θ in view of the simulated radar.

As in [12], $\mathbf{v_r}$ is obtained from the surface current field of ROMS as configured and run for [6]. This application of ROMS used a one-way nesting scheme and climatology [52], [53], with the two innermost domains forced by the Weather Research Forecast model at 6 km resolution

[54]. The surface velocity field, with 100m resolution, is used to compute the radial component to a simulated HF site ($\mathbf{v_r}$) for all of the $\mathcal{O}(1 \times 10^4)$ grid points within a range cell (e.g. Fig. 1), at several ranges. The radar simulations assume constant $\mathbf{v}_r$ in time (i.e. over all data snapshots). Fig. 2 shows the profiles of $\mathbf{v_r}$ used in radar simulations, which were limited to the six range cells shown, each originating from the same hour of ROMS data.

The model (7) includes a random factor $\boldsymbol{\gamma}_\pm$ to decorrelate the signals at an angular separation below the angular resolution of the radar [12]. The simulation constructs the $N \times N$ matrix $\boldsymbol{\gamma}_\pm$ from an $N \times 1$ vector of zero mean random numbers drawn from a normal distribution (defined here as the vector $\gamma_\pm$), such that $\boldsymbol{\gamma}_\pm = diag(\gamma_\pm)$, where the $diag$ function maps the vector to the diagonal of a matrix. New values for $\gamma_\pm$ are drawn for each data snapshot. The matrix $\boldsymbol{\gamma}_\pm$ models an ocean surface processes that results in uncorrelated HF radar data for angular separations of about $0.5^o - 2^o$ [17], [26], [55]. Previous simulation-based studies included the effect of wind [26]–[29], some using it to decorrelate signals in the way that (7) uses $\boldsymbol{\gamma}_\pm$ [26], [27]. Rather than include the additional complexity of wind effects on the angular distribution of Bragg waves, the model specified by (7) assumes the homogeneous presence of Bragg waves (both advancing and receding) at all θ.

Using (7) in (3) produces voltage timeseries that contain the combined signal for the frequencies given by $\pm\omega_B + \boldsymbol{\omega}_c$. Following the processing scheme described in section II, the auto and cross spectra of these timeseries are computed and K of them averaged together (which is equivalent to forming averaged cross spectra (CSS) in the SeaSonde). We then populate a covariance matrix $\mathbf{C}(f)$ for each frequency bin separately. $\mathbf{C}(f)$ forms the input to the DOA methods.

IV. Direction of Arrival Methods

Of the many alternative methods to MUSIC for DOA processing, several appear suitable for application to oceanographic HF radar based on their reported performance characteristics. The following reviews the MUSIC algorithm, prior to describing alternative DOA methods and their differences.

A. Multiple Signal Classification

The MUSIC algorithm [13]–[16] was a major advance for problems requiring determination of the DOAs of multiple simultaneously incident sources. These problems arise in many branches of science and technology including seismology, astronomy, sonar, bomb detection, personal communications, and medical research [24], [56].

Beginning with the eigen-decomposition of the data covariance matrix $\mathbf{C}$, the MUSIC algorithm associates the N largest eigenvalues with the signal and the remaining $M-N$ eigenvalues with the noise. The eigenvectors associated with the signal form the signal subspace $\mathbf{E}_S$ and those associated with the noise form the noise subspace $\mathbf{E}_N$. From $\mathbf{E}_N$ MUSIC computes the DOA function $P_{MUSIC}(\theta)$ for each θ in $\mathbf{A}$ as:

$$P_{MUSIC} = \frac{1}{\mathbf{A}^H \mathbf{E}_N \mathbf{E}_N^H \mathbf{A}}, \tag{8}$$

where $\mathbf{A}(\theta)$ is $M \times 1$. The DOA solutions are the θ_N found at peak values of (8). The advantage of MUSIC is that the search over all θ is 1-D.

B. Weighted MUSIC

Introducing a weighting matrix $\mathbf{W}$ into the MUSIC DOA function creates the DOA method known as Weighted MUSIC (W-MUSIC; [24]). The weighting matrix modifies the relative influence of each of the eigenvectors, with the goal of improving angular resolution without increasing error:

$$P_{W-MUSIC} = \frac{1}{\mathbf{A}^H (\mathbf{E}_N \mathbf{E}_N^H) \mathbf{W} (\mathbf{E}_N \mathbf{E}_N^H) \mathbf{A}}. \tag{9}$$

Investigations of W-MUSIC define $\mathbf{W}$ as $\mathbf{W} = \begin{bmatrix} 0 & 0 & 1 \end{bmatrix}^T \begin{bmatrix} 0 & 0 & 1 \end{bmatrix}$ (e.g. for the 3 element SeaSonde case), with the superscript T denoting transpose. With this definition of $\mathbf{W}$, W-MUSIC is known as the Min-Norm method [24]. The Min-Norm version of W-MUSIC exhibits improved performance at low SNR and small samples, and better resolution for uniform linear arrays [24].

C. Maximum Likelihood Estimation by Alternating Projection

Maximum Likelihood Estimation (MLE) methods in general produce the 'optimal' DOA solution, but due to their computational costs are rarely used in practice [56]. In the formulation

of [1], the MLE is computed with Alternating Projection search (MLE-AP), seeking the θ_N that maximize:

$$P_{MLE} = \mathrm{Tr}(\mathbf{A}(\mathbf{A}^H\mathbf{A})^{-1}\mathbf{A}^H\mathbf{C}), \tag{10}$$

where Tr is the matrix trace operator, and $\mathbf{A}$ is $M \times N$ as in (4). The MLE-AP algorithm [1] reduces the costs of computing (10) through an efficient search method. To search the N-dimensional solution space, the method alternately fixes one parameter (e.g. $\mathbf{a}(\theta_i)$ in $\mathbf{A}$), while maximizing the other (θ_j), until the overall maximum is obtained. As the algorithm steps through θ, rather than compute the projection $\mathbf{A}(\mathbf{A}^H\mathbf{A})^{-1}\mathbf{A}^H$ in (10), which includes a matrix inversion, the method uses a projection update formula to further reduce computational cost.

MLE-AP results in a substantial improvement in computational burden over MLE computed with other search methods - though it is still more demanding than MUSIC. This formulation of the maximum likelihood method is also known as the conditional maximum likelihood [25], and the deterministic maximum likelihood [24]. These definitions imply specific initial assumptions in the derivation of (10) - essentially that the signals are nonrandom but unknown. MLE-AP has been demonstrated to have lower errors and better angular resolution than MUSIC in a variety of scenarios [1], [24], [56].

D. Stochastic Maximum Likelihood

Derivation of the Stochastic Maximum Likelihood (SML) method starts with the initial assumption that the signals result from a Gaussian random process [57]. The derivation then results in a cost function that differs from (10). Instead the SML method finds the minimum of:

$$P_{SML} = \log(\det(\mathbf{A}(\mathbf{A}^\dagger(\mathbf{C} - \sigma\mathbf{I})\mathbf{A}^{\dagger H})\mathbf{A}^H + \sigma\mathbf{I})). \tag{11}$$

Where σ is defined,

$$\sigma = \frac{1}{M-N}\,\mathrm{Tr}((\mathbf{I} - \mathbf{A}\mathbf{A}^\dagger)\mathbf{C}). \tag{12}$$

Here $\mathbf{I}$ is the $M \times M$ identity matrix, and $\mathbf{A}^\dagger$ is the Moore-Penrose inverse of $\mathbf{A}$. Our implementation of the SML method uses alternating projection search as in (10), but requires substantially more computational effort than MLE-AP due to the need to evaluate (11) at every step. Better performance for SML compared to other MLE methods has been observed for scenarios with low SNR or 'small' M [57].

E. Weighted Subspace Fitting

The Weighted Subspace Fitting method (WSF; [58]), alternatively known as the Method of Direction Estimation (MODE; [25], [59]), can be interpreted as an MLE method that fits the optimal subspace (e.g. spanned by $\mathbf{A}$) to the signal eigenvectors of $\mathbf{C}$ [25]. Beginning with an estimate of the noise variance from the noise eigenvalues λ_i of $\mathbf{C}$,

$$\sigma = \frac{\sum_{i=N+1}^{M} \lambda_i}{M - N}, \tag{13}$$

we compute the optimal weights with the matrix of signal eigenvalues $\mathbf{\Lambda}_S$:

$$\mathbf{W} = (\mathbf{\Lambda}_S - \sigma\mathbf{I})^2 {\mathbf{\Lambda}_S}^{-1}. \tag{14}$$

The WSF method then finds the minimum of the function:

$$P_{WSF} = \mathrm{Re}(\log(\mathrm{Tr}((\mathbf{I} - \mathbf{A}\mathbf{A}^{\dagger})\mathbf{E}_S\mathbf{W}\mathbf{E}_S^H))). \tag{15}$$

Similar performance has been found for WSF when compared to SML, with reduced computational cost [24]. WSF also provides a method for determining the number of signals [58] - a feature not investigated here.

Implementations of the above methods were validated with test scenarios using (3), and by reproducing figures from the cited publications. An additional test was formulated based on a detailed example SeaSonde simulation [40]. Results were also compared with the Cramer-Rao Lower Bound (CRB) [25], [44], [51], which gives the theoretical bound on the accuracy of an estimator based on the characteristics of the receive array, SNR, K, and N. Methods for computing the CRB are given in [12].

V. Receive Array Descriptions

This analysis evaluates DOA methods with the receive array types that are most frequently used to observe ocean surface currents. The array types include the SeaSonde (with $M = 3$), a rectangular array with $M = 8$ (hereafter RA-8), and a uniform linear array with $M = 16$ (hereafter ULA-16). The following describes each of the arrays with their 'idealized' mathematical characteristics, without considering the distortions from ideal that are typically encountered in the field. Array geometry fundamentally affects DOA performance and provides one aspect of the specific application in which to evaluate the DOA methods.

The SeaSonde array consists of three collocated antennas: a monopole and two orthogonal mounted loops [60]. The cosine response of the loop antennas gives the array its directional characteristics, while the monopole gives the phase and amplitude reference for normalization. The manifold matrix $\mathbf{a}(\theta)$ is given by,

$$\mathbf{a}(\theta) = \begin{bmatrix} \cos\theta & \sin\theta & 1 \end{bmatrix}^T. \tag{16}$$

The idealized representation of (16) consists solely of real valued numbers, since the phases are zero.

Given the increased oceanographic use of rectangular receive arrays (c.f. [61]), the following defines the RA-8 based on a 9-element, 3×3 square grid. Here the diagonal length of the square is set to λ_{TX}, such that the spacing between elements is $\lambda_{TX}/(2\sqrt{2})$. The diagonal of the grid is aligned parallel to the coastline, and the element nearest the ocean is removed. The mathematical description of the array begins with the definition of a uniform rectangular array (e.g. [25]),

$$\mathbf{a}(\theta) = \begin{bmatrix} \vdots \\ exp(i2\pi d(\mathbf{n}\cos(\theta) + \mathbf{m}\sin(\theta))) \\ \vdots \end{bmatrix}. \tag{17}$$

The grid spacing normalized by λ_{TX} is defined as $d = 1/(2\sqrt{2})$. Vectors $\mathbf{n}$ and $\mathbf{m}$ specify the element positions relative to the phase reference in the center of the array, defined $\mathbf{n} = [0 \quad 1 \quad -1 \quad 0 \quad 1 \quad -1 \quad 0 \quad 1]^T$, and $\mathbf{m} = [-1 \quad -1 \quad 0 \quad 0 \quad 0 \quad 1 \quad 1 \quad 1]^T$. The element with $n = m = -1$ has been removed, giving a total of $M = 8$ elements.

Following [56], the ULA-16 is defined with θ relative to the array normal, $\lambda_{TX}/2$ spacing between elements, and phases referenced to the center of the array,

$$\mathbf{a}(\theta) = \begin{bmatrix} exp(i2\pi d_1 \sin\theta) \\ \vdots \\ exp(i2\pi d_M \sin\theta) \end{bmatrix}. \tag{18}$$

In (18), d_m, with $m = \{0, 1, ..., M-1\}$ specifies the distance from the array center,

$$d_m = \frac{1}{2}(m - \frac{M-1}{2}). \tag{19}$$

A linear array with $\lambda_{TX}/2$ spacing is known as a uniform linear array [25].

VI. Additional Simulation Methods

A. Empirical Signal Detection

The determination of the number of signal sources, known as signal detection, typically forms an integral aspect of the DOA calculation, directly influencing the performance of the radar. Detection methods commonly used with direction finding oceanographic HF radars [33] depend in part on parameters that are specific to MUSIC processing, namely the eigenvalues and their ratios. A preliminary analysis of detection methods highly cited in the DOA literature (e.g. the Akaike Information Criteria (AIC) and Minimum Description Length (MDL) [45]) suggests that these methods are not suitable for oceanographic radars. These methods rely on large differences between signal eigenvalues and noise eigenvalues, while eigenvalues from oceanographic radars often have small differences – leading to errors in detection. Further work to identify suitable detection methods for oceanographic radars, particularly ones that do not depend on the distribution of eigenvalues, is ongoing. In the meantime, in order to isolate performance specific to the DOA method, this analysis specifies the number of signal sources based on the ROMS ocean current fields input to the simulation. Considering the DOA methods in isolation allows the analysis of relative performance based solely on the DOA method, removing additional performance factors that may result from imperfect signal detection.

The goal of signal detection is to identify the number of distinct signal sources (N) that are represented by the data covariance matrix. The DOA inversion then uses N and the covariance matrix to find the bearings to the signal sources. Since the simulation uses a known current field as the input, this information can be used to specify N. Fig. 2 shows the profiles of $\mathbf{v}_r$ from ROMS used in the radar simulations, plotted as a function of bearing, along with the empirically determined values of the number of signal sources (N) for different values of $\mathbf{v}_r$. The choice of N necessitates some subjectivity, since the radars ability to resolve separate signal sources is a function of the array beamwidth, the SNR, and the source separation (c.f. Appendix B of [12], and [44]).

When simulation inputs consist of surface currents from ROMS, a 'signal source' consists of an area of grid of points that span a range of bearings with similar values of $\mathbf{v}_r$ (i.e. values of $\mathbf{v}_r$ in the same Doppler bin). The area of grid points, or spatial patch, spans 1.5 km in range, and some angular width, which varies significantly as shown by Fig. 2. For example, the region

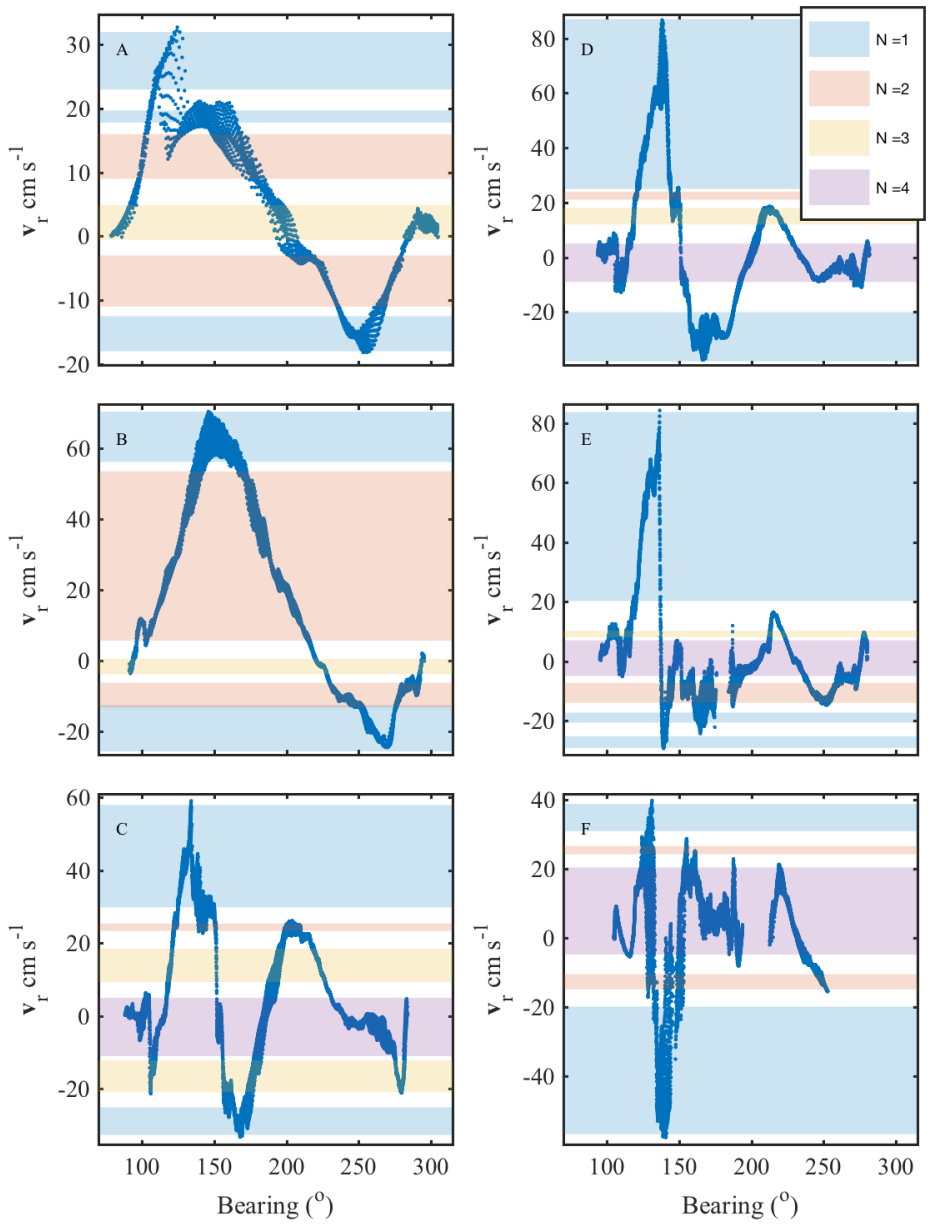

Fig. 2. Profiles of $\mathbf{v}_r$ from ROMS used in radar simulations, with counts of source patches (N) shown by colored regions (see legend), for range cells a) 4.0 km, b) 11.5 km, c) 29.5 km, d) 34 km, e) 38.5 km, and f) 53.5 km

in Fig. 2a, with $\mathbf{v}_r \sim 19$ cm s^{-1} spans bearings between 100^o and 165^o. Very narrow angular widths, such as in Fig. 2c, with $\mathbf{v}_r$ near ~ 19 cm s^{-1} and bearing near 160^o are also found. The latter appear to be missed by DOA methods, mostly likely due to the low SNR they produce. By inspection of these figures, regions of $\mathbf{v}_r$ are associated with $N = 1$, $N = 2$, $N = 3$, or $N = 4$ sources as shown by the colored regions in the figures. Regions shown in Fig. 2 were used in the SeaSonde and RA-8 simulations, with slightly different values for N used with the ULA, due to the narrower field of view (98^o-276^o) for that array.

B. Monte Carlo Simulations

For both the discrete source simulations and the oceanographic radar simulations with ROMS, 400 Monte Carlo simulations are run for each integer SNR from 0 to 30 dB. For each iteration, new random values for noise are generated at the specified SNR. The oceanographic radar simulations use a limited number of ROMS range cells, shown in Fig. 2, due to the need to empirically determine the effective number of signal sources (i.e. spatial patches of signal with similar Doppler velocity) as described above. Though limited in number, these range cells provide a thorough evaluation of the DOA methods. The ROMS range cells present the DOA methods with N in the range $1 < N < 4$, with a variety of angular separations between them, and with variation in the angular widths of each signal source spatial patch. Thus the analysis explores a parameter space defined by SNR, N, the angular separation between sources, and the angular widths of each source patch – for a variety of receive arrays and DOA methods.

C. RMS Error Calculation

One metric used to evaluate DOA method performance is the RMS bearing error, σ_{RMS}. Given the simulation source locations at θ_i, the DOA estimates $\hat{\theta}_i$ from a DOA method, and an ensemble size n, σ_{RMS} is computed,

$$\sigma_{RMS} = \sqrt{\frac{\sum_{i=1}^{n}(\theta_i - \hat{\theta}_i)^2}{n}}. \tag{20}$$

When using $\mathbf{v}_r$ from ROMS, the signal source represented by θ_i takes on a range of possible values as described above. In this case, the value of θ_i that is closest to $\hat{\theta}_i$ is used when computing (20).

D. SNR Calculation

In simulations with the discrete source model, SNR is defined as,

$$SNR = 10log_{10}(\sigma_s)/\sigma_n), \tag{21}$$

where σ_s and σ_n are the variance of the array voltage and noise respectively, as defined for (3). When simulating oceanographic radars, the SNR calculation follows the SeaSonde method (c.f. [62]), where (21) is computed using the bin value of the power spectrum for σ_s, and σ_n is estimated from an average of the noise-only Doppler bins, outside of the region expected to contain Bragg scattered signal.

VII. RESULTS

The following describes results of simulations using (3), first with discrete sources model (6), and then with the oceanographic radar model (7) and $\mathbf{v}_r$ from ROMS. Beginning with the discrete source model allows us to demonstrate known differences in DOA methods for ULAs, and then look for these differences with the SeaSonde and RA-8. We also use the discrete source model to investigate the SeaSonde with $N = 3$, which may occur with oceanographic radars as suggested by ROMS $\mathbf{v}_r$. The results of simulations with the discrete source model inform the interpretation of the more complex simulations using the oceanographic radar model.

A. Discrete Sources at Two Bearings

To illustrate known performance differences between the DOA methods, we first simulate two discrete, closely spaced signal sources, following a scenario described in [25]. The scenario, simulated here with the ULA-16, $K = 10$, and SNR ranging from 0 to 30 dB, illustrates a characteristic of MUSIC known as MUSIC-breakdown, which is defined as an abrupt loss of accuracy below a given SNR threshold [63], [64]. Simulations using two sources separated by $\Delta\theta = 3.2^o$ produce a substantial increase in σ_{RMS} for MUSIC and W-MUSIC compared to WSF, SML and MLE-AP (Fig. 3) with decreasing SNR. In this scenario, the source spacing is a fraction of the array half power beamwidth ($\Delta\theta_{HPBW}$). As $\Delta\theta_{HPBW}$ typically represents the resolution of beam forming radars, this scenario demonstrates the SNR required to resolve sources with "super-resolution" [44] – or the ability to distinguish signal sources separated by less than the beamwidth. Here $\Delta\theta_{HPBW}$ is computed as the range of θ where the power of the

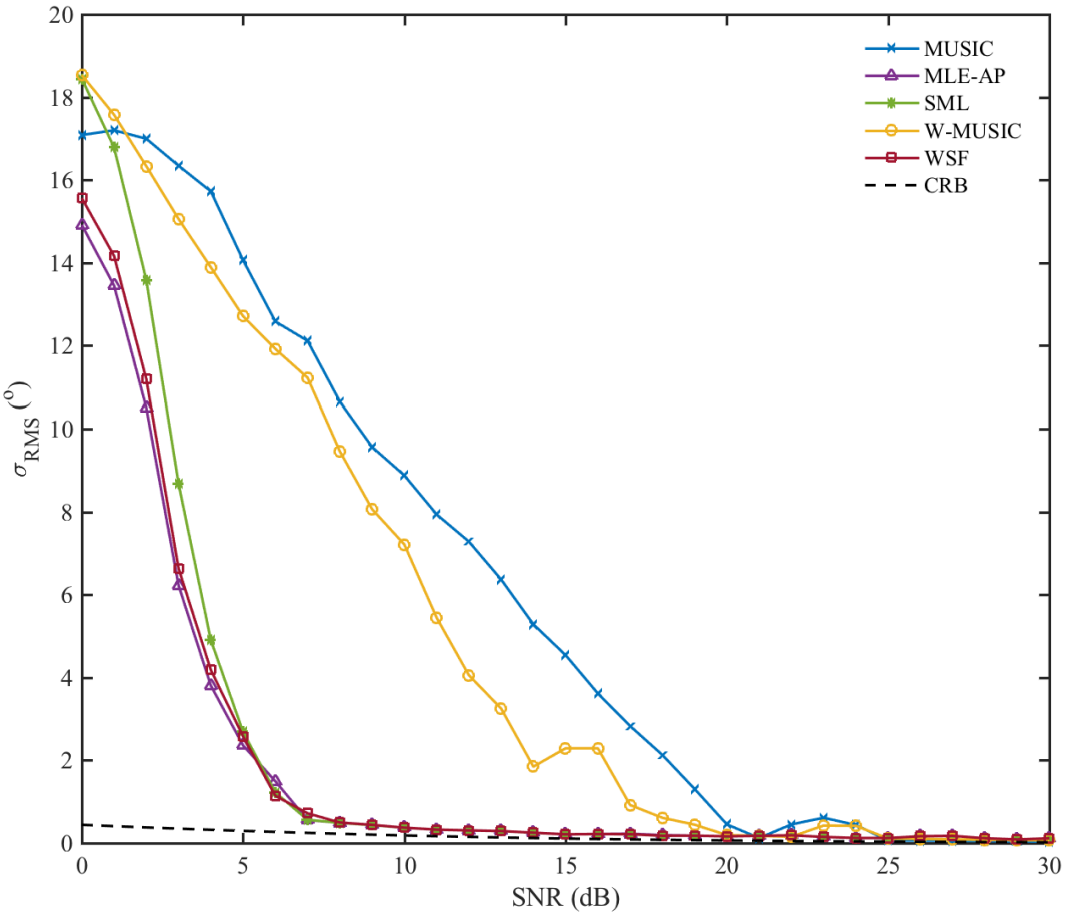

Fig. 3. σ_{RMS} vs. SNR for the DOA methods, from simulations of two signal sources separated by 3.2^o, for a 16-element linear array with $K = 10$ as demonstrated in [25]. The CRB is shown for comparison.

main beam is greater than half the maximum power (c.f. [25]). Given the array manifold, the antenna power is computed,

$$P(\theta) = \left| \frac{1}{M} \mathbf{A_0}^H \mathbf{A}(\theta) \right|^2, \tag{22}$$

where $\mathbf{A_0} = \mathbf{A}(\theta_0)$ given the reference angle θ_0 ($\theta_0 = 0^o$ here). For example, the ULA-16 has $\Delta\theta_{HPBW} = 6.37^o$, and the test scenario has sources separate by $\Delta\theta_{HPBW}/2$.

MUSIC-breakdown is well known for standard array types such as ULAs [25], [63], [64], but it is not known to have been investigated for the SeaSonde. Fig. 4a shows results of simulations with the SeaSonde array and sources located at $\Delta\theta = 65.5^o$, or about half the SeaSonde $\Delta\theta_{HPBW} =$

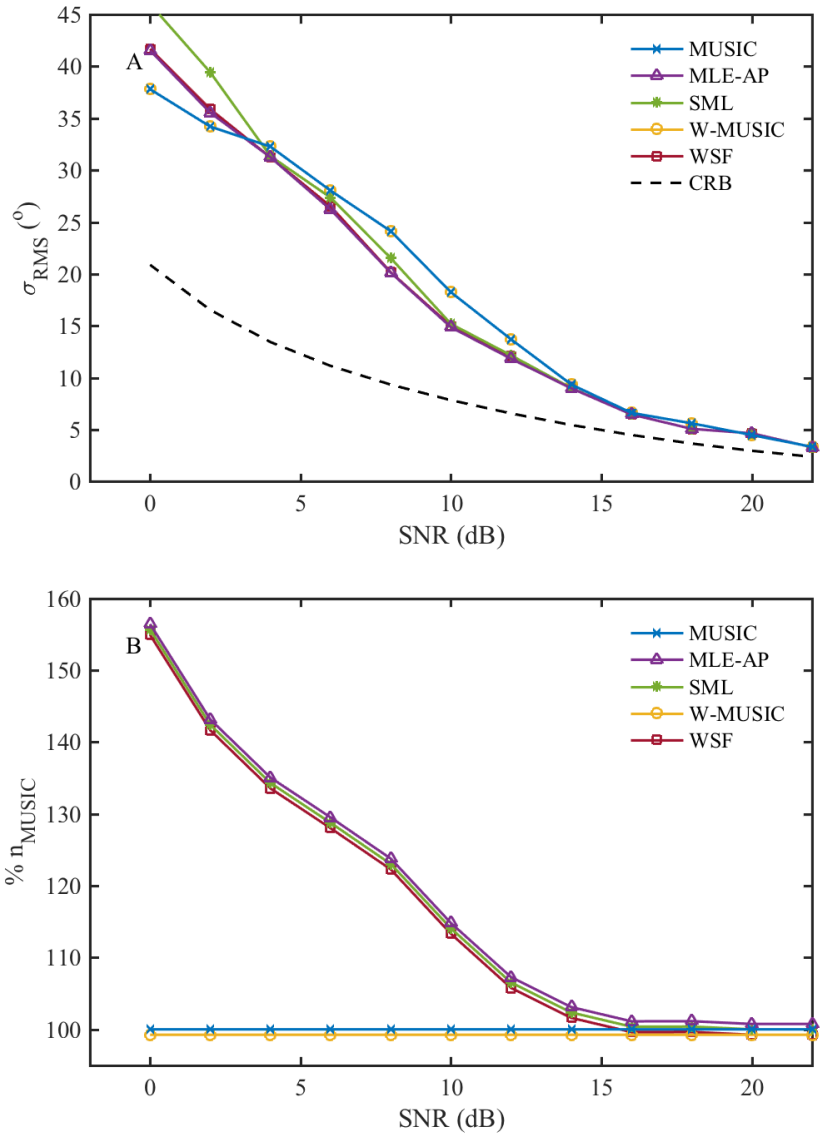

Fig. 4. a) σ_{RMS} vs. SNR for the DOA methods from simulations of two signal sources separated by 65.5^o (0.5 $\Delta\theta_{HPBW}$), for a 3-element SeaSonde array with $K = 10$. b) The number of DOA solutions returned by each method, expressed as a percentage of the solutions returned by MUSIC computed with (23). WSF, MLE-AP and W-MUSIC have been slightly offset for clarity.

131^o. MUSIC-breakdown is not observed for the SeaSonde. Instead Fig. 4a shows similar σ_{RMS} for all DOA methods, with MLE-AP, SML and WSF showing only slightly lower σ_{RMS} between 5-13 dB SNR. Below 4 dB SNR, σ_{RMS} for all methods becomes greater than half the source separation (or greater than 32^o).

In simulations with the SeaSonde, instead of MUSIC-breakdown (i.e. in accuracy), as SNR decreases MUSIC increasingly fails to resolve the two sources. MUSIC and W-MUSIC instead return single DOA solutions, while MLE-AP, WSF and SML consistently return two solutions. Since we are interested in performance relative to MUSIC, Fig. 4b shows the fraction of DOA solutions returned expressed as a percentage of the number returned by MUSIC,

$$\% \; n_{MUSIC} = \frac{n}{n_{MUSIC}} * 100. \tag{23}$$

Below 15 dB SNR, the number of DOA solutions from MLE-AP, WSF and SML exceed those of MUSIC and W-MUSIC, increasing linearly with decreasing SNR.

Other effects of signal source separation on DOA performance with the SeaSonde array are shown by Figs. 5 and 6. Simulations for these figures again used two sources, but at separations of $0.3 * \Delta\theta_{HPBW} = 39.3^o$ and $0.7 * \Delta\theta_{HPBW} = 91.7^o$ respectively. The plot of σ_{RMS} vs. SNR in Fig. 5a shows higher σ_{RMS} for the more closely spaced signal sources when compared with Fig. 4a. In this case, MUSIC and W-MUSIC produce lower σ_{RMS} at low SNR compared with the other DOA methods, but as shown by Fig. 5b, these result from significantly fewer DOA solutions. As shown by Fig. 5b, MLE-AP, WSF, and SML return more than 140% of n_{MUSIC} between 5-10 dB. Simulations with sources separated by $0.7 * \Delta\theta_{HPBW}$ in contrast, show that increased separation results in similar σ_{RMS}, and diminished differences in $\% \; n_{MUSIC}$ between the DOA methods. Similar results were found when using the RA-8 array ($\Delta\theta_{HPBW} = 51.1^o$) in these scenarios. As the source spacing increases, the differences between the methods diminish. When sources are closely spaced, and the SNR is low, increased DOA solutions for MLE-AP, SML and WSF suggest that their use could increase the azimuthal resolution and coverage of oceanographic HF radars.

B. SeaSonde with Three Discrete Sources

The input velocity field from ROMS in Fig. 2 indicate the likelihood of situations with $N \geq M$ for the SeaSonde. This situation results when the same $\mathbf{v}_r$ occurs at more than $M - 1$ separate

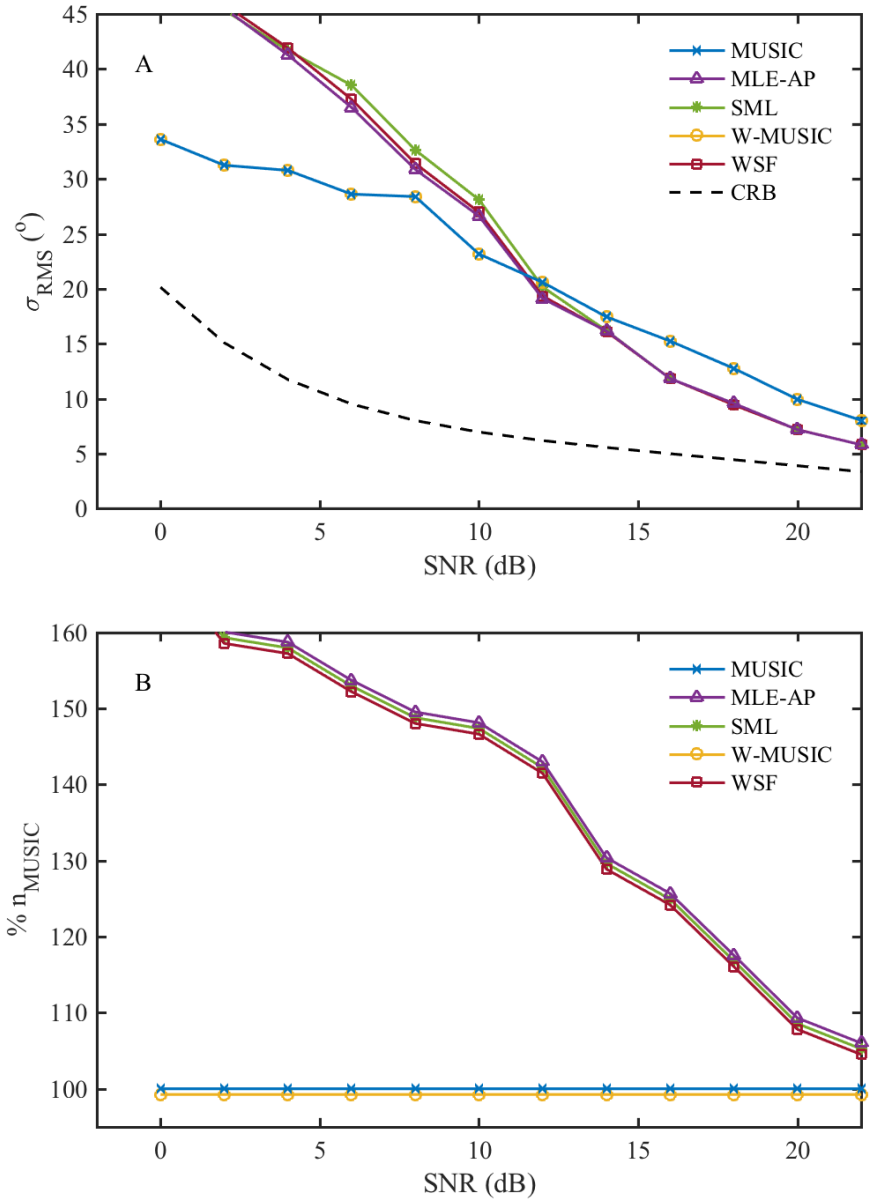

Fig. 5. a) As in Fig. 4a, for sources 39.3^o apart ($0.3\ \Delta\theta_{HPBW}$). b) As in Fig. 4b.

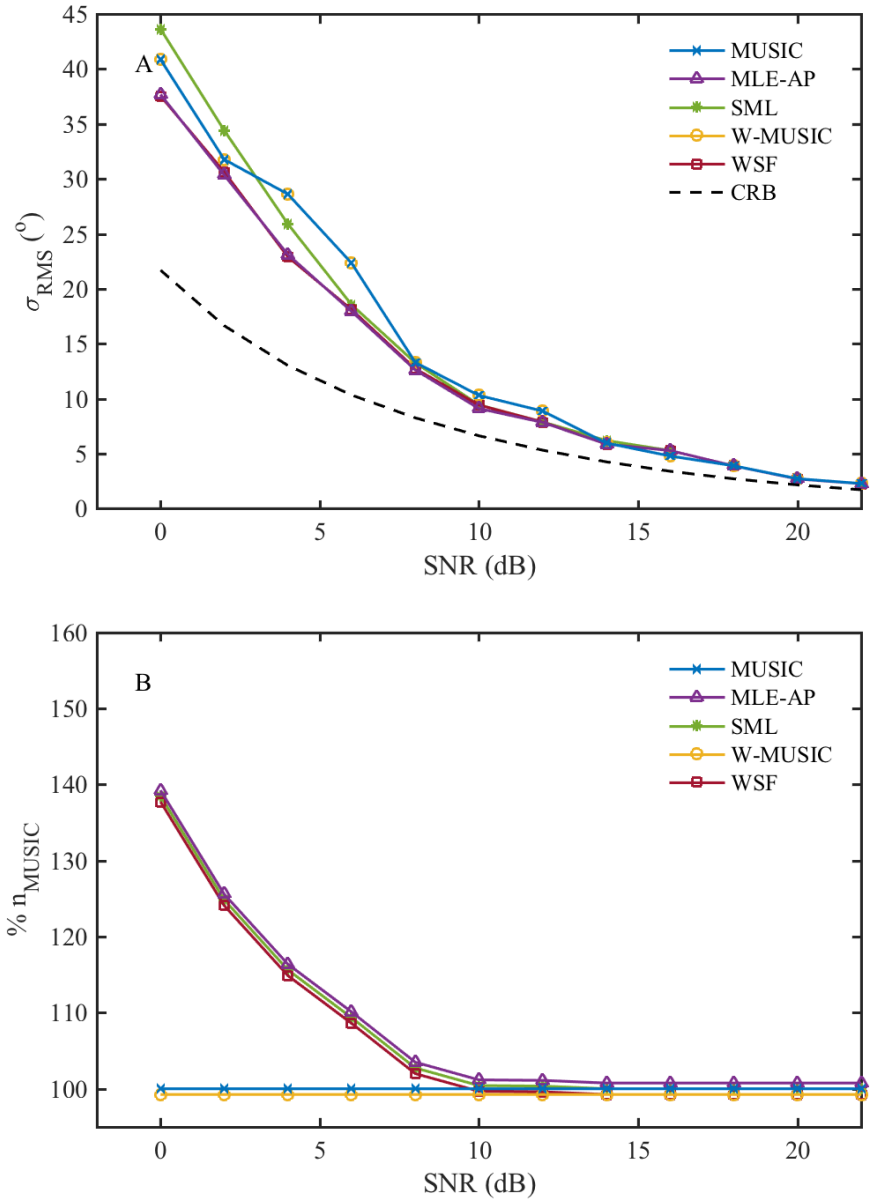

Fig. 6. a) As in Fig. 4a, for sources 91.7^o apart ($0.7\ \Delta\theta_{HPBW}$). b) As in Fig. 4b.

patches, for example in Fig. 2a for $0 < \mathbf{v}_r < 4$ cm s^{-1}. Given the likelihood of this scenario, simulations were run to investigate the effect on performance, and to identify any difference between DOA methods that may result.

Fig. 7 shows σ_{RMS} vs. SNR resulting from simulations with the SeaSonde and $N = 3$ discrete,

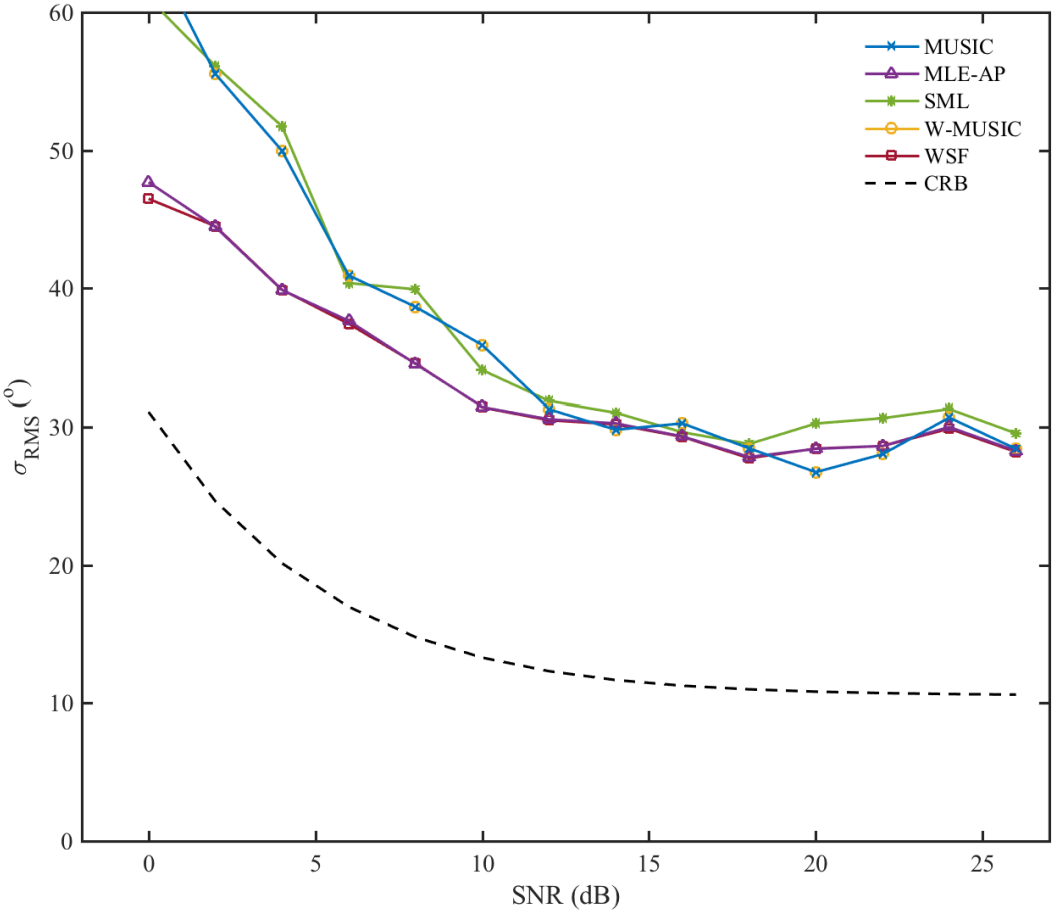

Fig. 7. σ_{RMS} vs. SNR for the DOA methods from simulations of 3 signal sources at -65^o, 0^o and 65^o, for an $M = 3$ element SeaSonde array with $K = 10$.

equal power sources located at -65^o, 0^o, and 65^o. The presence of the third signal source causes elevated σ_{RMS}, with minimum values near 30^o. Overall, σ_{RMS} is higher than found with the two source simulations (e.g. Figs. 4a, 5a, and 6a). Results from MLE-AP and WSF show slightly lower σ_{RMS} for SNR < 10 dB compared to MUSIC. Inspection of the individual DOA solutions

(not shown) suggest that the presence of the third signal source introduces error equally into the two DOA solutions.

The simulations of the SeaSonde with $N = 3$ demonstrate the influence of the presence of the third source on the DOA performance. In the case of MUSIC and W-MUSIC, the eigen decomposition of the data covariance matrix typically sorts the variance into orthogonal components consisting of signal and noise. In the $N = 3$ case, the eigen decomposition is unable to separate the signal and noise into separate subspaces, leading to errors in the DOAs returned by MUSIC. This phenomenon, known as subspace leakage [24], [56], occurs when the assumption that $N < M$ does not apply. DOA solutions from MLE-AP, WSF and SML are similarly corrupted in this situation, though the mechanism differs. Further simulations varying relative signal levels of the sources, along with Fig. 7, indicate that when the ocean surface presents $N \geq M$, the resulting DOA solutions will have higher σ_{RMS} than when $N < M$. Furthermore, when $N \geq M$, the $M-1$ solutions identified will result from the sources with the highest SNR, or the largest angular separation.

C. Sources Based on ROMS

1) SeaSonde Array: Figs. 8a-d show results obtained with the DOA methods when applied to simulations with ROMS $\mathbf{v}_r$ (Fig. 2). Results quantifying performance with σ_{RMS} are separated by the number of signal sources N as described above. When $N = 1$ (Fig. 8a) similar results are found for MUSIC, MLE-AP, and WSF, while higher σ_{RMS} is found for W-MUSIC, and for SML when $SNR > 20$ dB. The $N = 2$ results in Fig. 8b are similar to the results of Fig. 4a, with the exception of the high σ_{RMS} found for SML. In Figs. 8a-c, minimum values of σ_{RMS} increase with increasing N, as suggested by the results the simulations of $N = 3$ discrete sources. Minimum σ_{RMS} goes from less than 3^o when $N = 1$ (Fig. 8a), to $\sigma_{RMS} > 5^o$ when SNR< 20 dB and $N = 2$ (Fig. 8b), and up to 15^o when $N = 3$ (Fig. 8c). The decreased σ_{RMS} in Fig. 8d compared to the $N < 4$ cases results when the presence of the flow field at many bearings creates an upper limit on the maximum possible error. For example, in Fig. 2f with $0 < \mathbf{v}_r < 10$ cm s^{-1}, the angular distance between patches of $\mathbf{v}_r$ is at most 25^o. Overall, with the SeaSonde array Figs. 8a-d show very little difference in performance in terms of σ_{RMS} between MUSIC, MLE-AP, and WSF.

As suggested by Figs. 4b, 5b, and 6b, however, simulations with ROMS identify an advantage

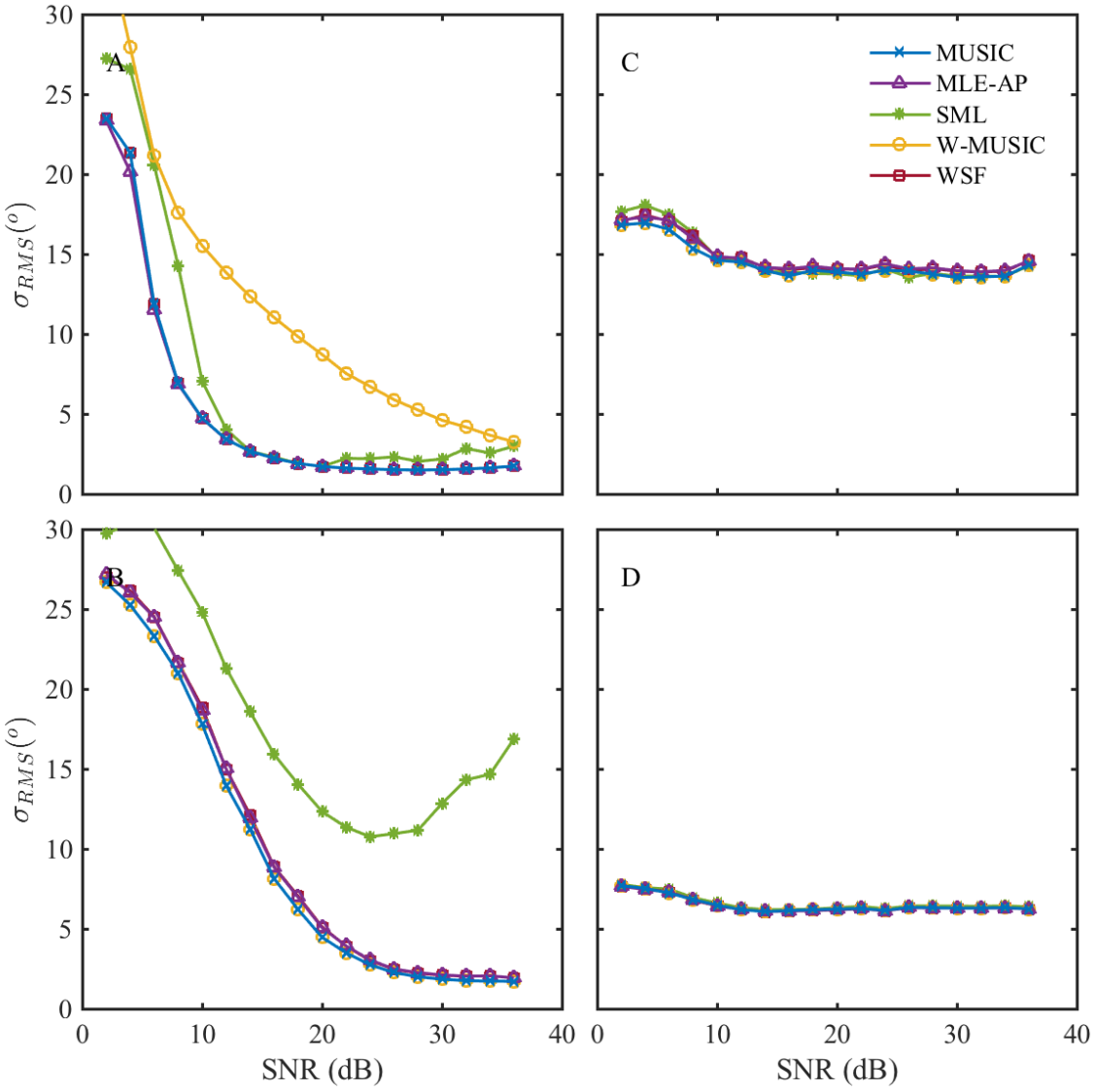

Fig. 8. σ_{RMS} vs SNR for simulations with the ROMS radial velocities in Fig. 2 and the SeaSonde receive array, for a) $N = 1$, b) $N = 2$, c) $N = 3$ and d) $N = 4$.

444 for MLE-AP and WSF in terms of the number of DOA solutions returned. Figs. 9a-d show the number of DOA solutions as a percentage of the number returned by MUSIC, $\%n_{MUSIC}$ as in

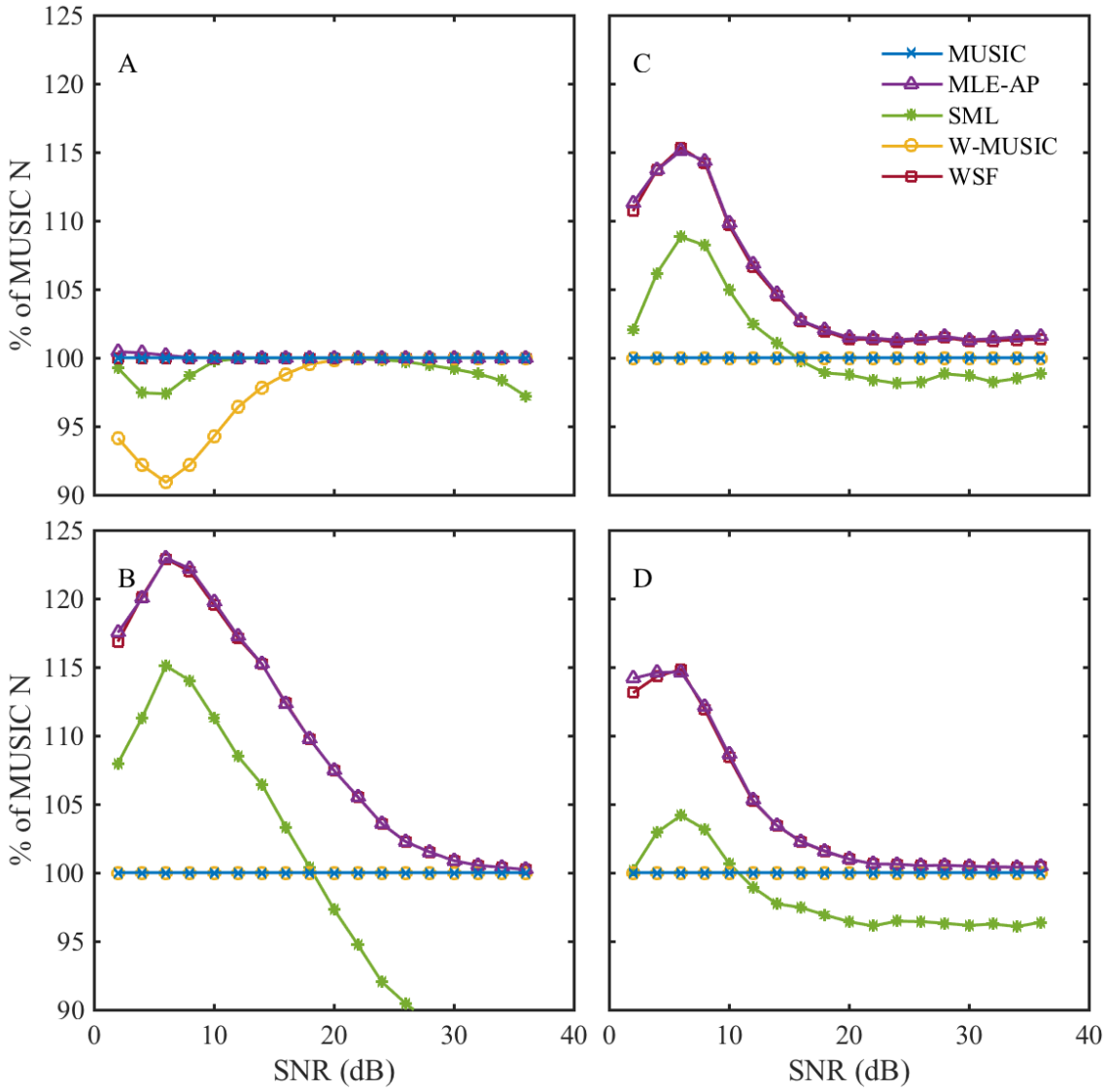

Fig. 9. Percent of MUSIC solutions vs. SNR for simulations with the ROMS radial velocities in Fig. 2 and the SeaSonde receive array, for a) $N = 1$, b) $N = 2$, c) $N = 3$ and d) $N = 4$.

445

446 (23), separating the results by the number of sources and plotting vs. SNR. When $N = 1$, MUSIC,
447 MLE-AP and WSF perform similarly, with a slight advantage over SML and W-MUSIC. In the

$N = 2$ case (Fig. 9b), MLE-AP and WSF produce more than 120% of n_{MUSIC} at low SNR. Figs. 9c and d show similar results, with MLE-AP and WSF producing up to 115% of n_{MUSIC}. The improvement in $\%n_{MUSIC}$ occurs when $N > 1$, with most occurring when $SNR < 20$ dB, and the largest differences occurring just below 10 dB.

2) Rectangular 8 Element Array: Figs. 10a-d summarize results of simulations with ROMS and the RA-8 receive antenna, in terms of σ_{RMS} as in Figs. 8a-d. Fig. 10a with $N = 1$ shows similar performance for all the DOA methods, with $\sigma_{RMS} < 3^o$ for $SNR > 10$ dB. This result contrasts with Fig. 10b, which shows a significant difference between the DOA methods for $N = 2$. The early "breakdown" in MUSIC performance occurs near $SNR = 20$ dB (for both MUSIC and W-MUSIC), with MLE-AP, WSF and SML producing σ_{RMS} near 1^o for SNR as low as 12 dB. Maximum values of $\sigma_{RMS} = 8^o$ for MLE-AP occur at 4 dB SNR. The DOA methods produce similar results for $N = 3$ and $N = 4$ (Figs. 10c and 10d), with low σ_{RMS} at low SNR for all DOA methods in Fig. 10d. As in Fig. 8d, this results from the presence of the flow at many bearings creating an upper limit on the maximum possible error. Fig. 10c shows a $1^o - 2^o$ advantage in σ_{RMS} for MUSIC, which results from fewer data points as shown by Figs. 11c and 11d. These figures show $\%n_{MUSIC}$ for the RA-8 simulations, with MLE-AP and WSF producing up to 120% and 140% of n_{MUSIC} for $N = 3$ and $N = 4$.

3) Linear 16 Element Array: Figs. 12a-d show σ_{RMS} for simulations with ROMS and the ULA-16. A difference between MUSIC, MLE-AP and WSF occurs when $N = 2$ (Fig. 12b), which shows σ_{RMS} near 6^o for MUSIC, 4^o for WSF, and 3^o for MLE-AP. Similar, though diminished differences occur in Figs. 12c and 12d. All the methods return the same number of DOA solutions (data not shown). Compared with the other arrays, the ULA-16 produces very low σ_{RMS}. Fig. 12a has the lowest values of σ_{RMS} for any of the receive arrays, less than 1^o, for SNR> 10 dB, computed over its narrower azimuthal of view.

4) Computational Cost: Table I summarizes the computational costs for the DOA methods and the three receive arrays, as the time relative to MUSIC. Times were logged for each of the DOA methods over the 8800 simulations per ROMS range cell, with the count incrementing only when the DOA method was running. To produce Table I, total time for each method was divided by the time used by MUSIC. Results demonstrate the well known computational advantage for MUSIC (and W-MUSIC), approximately a factor of 10, compared to MLE-AP. SML and WSF require considerably more computational time. As implemented, MLE-AP uses the projection

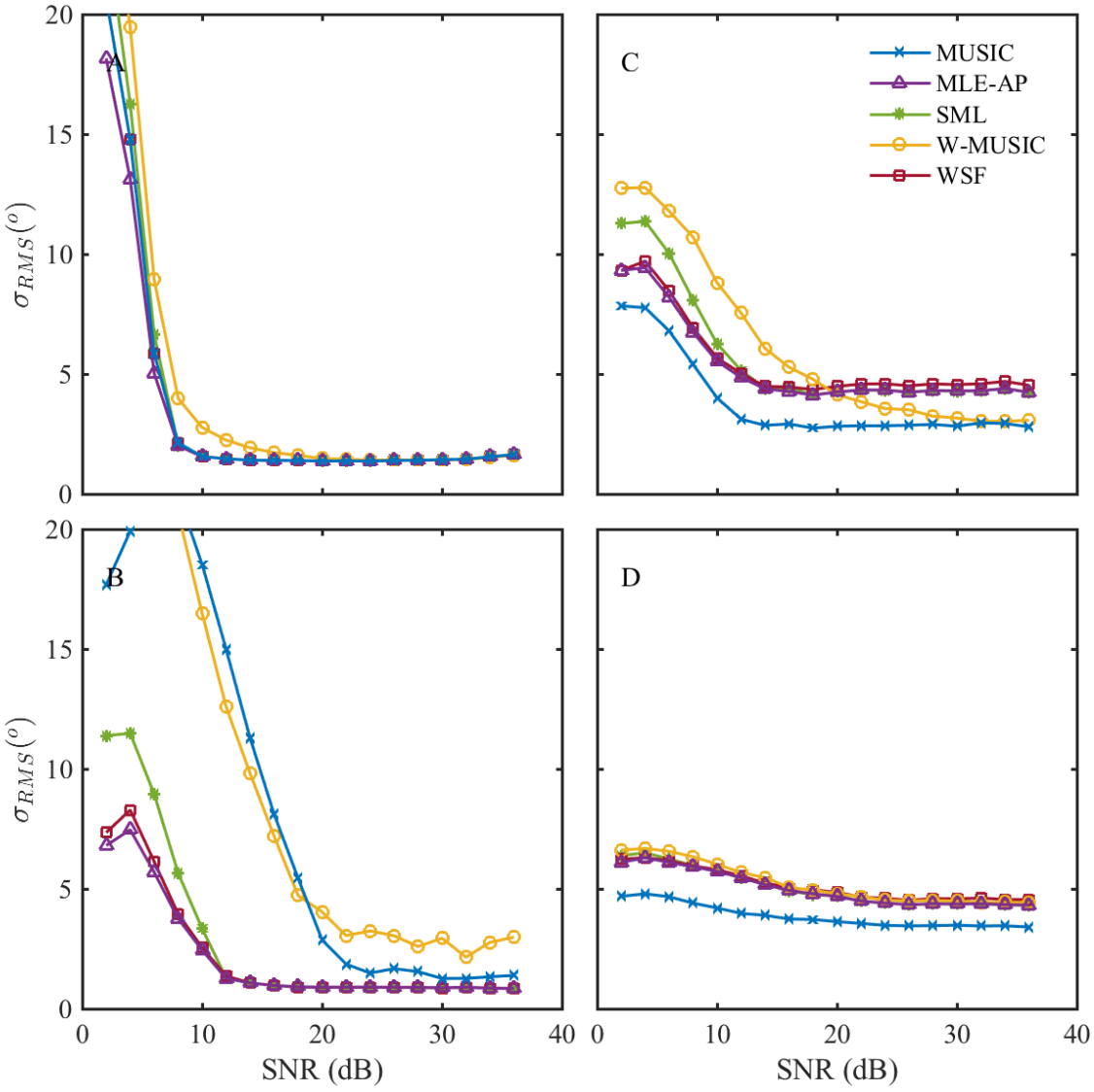

Fig. 10. σ_{RMS} vs SNR for simulations with ROMS radial velocities in Fig. 2 and the 8-element rectangular array (RA-8), for a) $N = 1$, b) $N = 2$, c) $N = 3$ and d) $N = 4$.

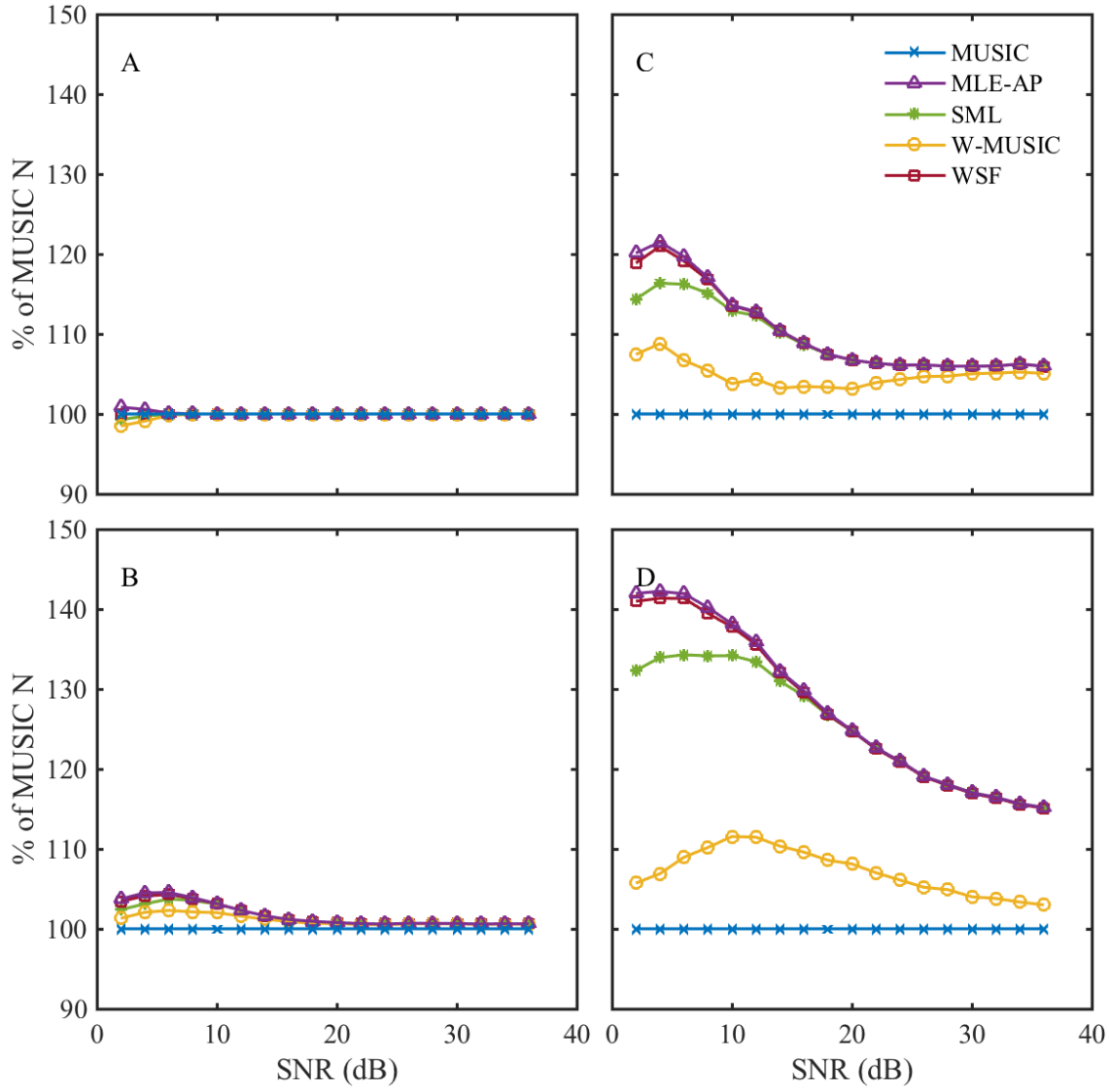

Fig. 11. Percent of MUSIC solutions vs. SNR for simulations with the ROMS radial velocities in Fig. 2 and the 8-element rectangular array (RA-8), for a) $N = 1$, b) $N = 2$, c) $N = 3$ and d) $N = 4$.

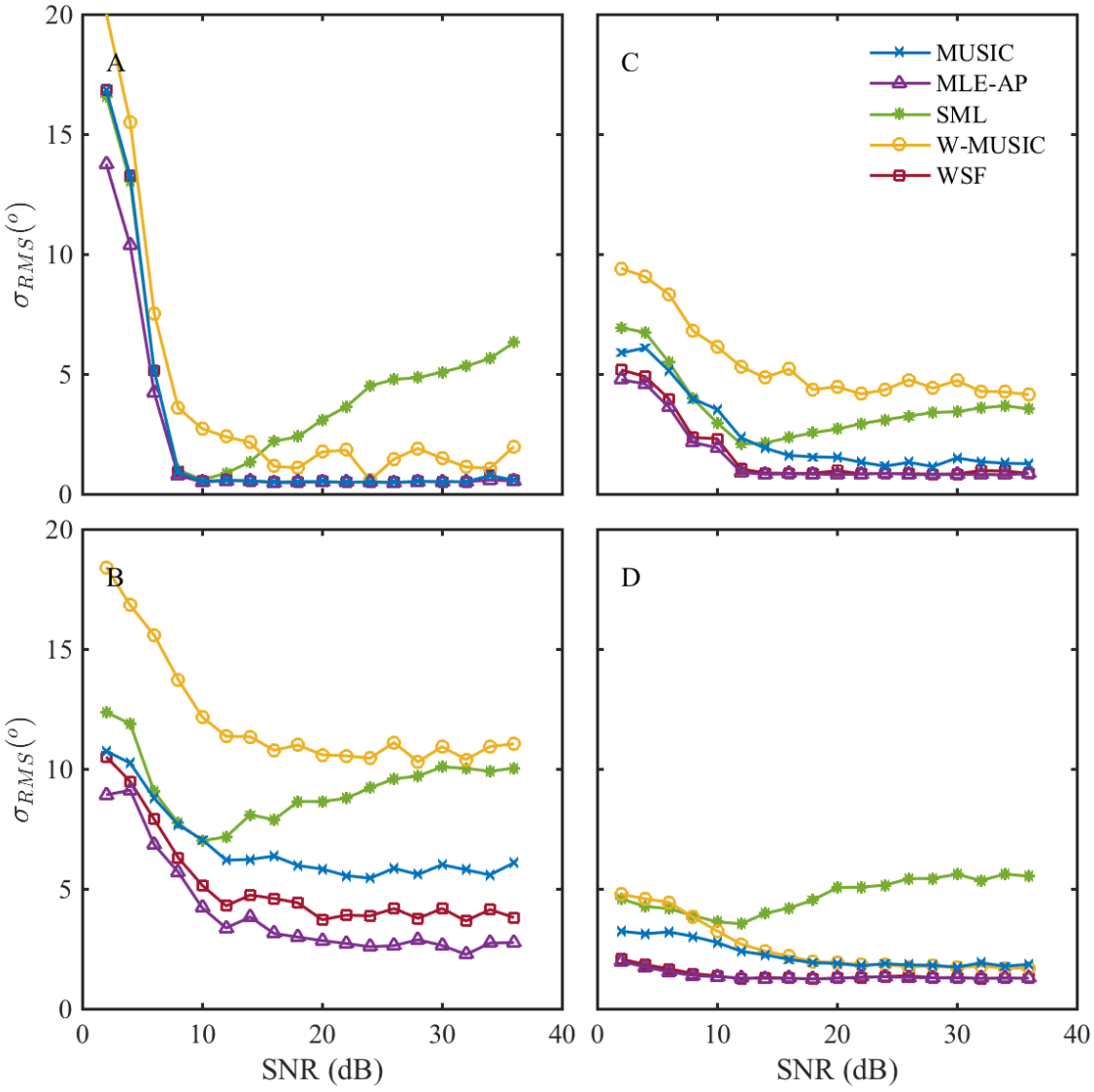

Fig. 12. σ_{RMS} vs SNR for simulations with ROMS radial velocities in Fig. 2 and the 16 element linear array (ULA-16), for a) $N = 1$, b) $N = 2$, c) $N = 3$ and d) $N = 4$.

update formula [1], which significantly decreases the computational demands relative to SML and WSF, both of which use the alternating projection search described for MLE-AP [1]. Table I reports the relative times, since actual run times varied by orders of magnitude depending on the computer used, while the relative times were found to be stable. As an example, processing time on a desktop computer with 16 GB RAM and a 3.4GHz processor for 4600 Doppler bins (approximately the size of a typical SeaSonde Cross Spectra file for all range cells) with the SeaSonde array, was about 15 s for MUSIC, and 116 s for MLE-AP (implemented in MATLAB).

DOA Method	SeaSonde	RA-8	ULA-16
MUSIC	1.0	1.0	1.0
W-MUSIC	1.6	1.7	1.8
MLE-AP	8.0	15	11
WSF	23	52	31
SML	30	71	42

TABLE I. COMPUTATIONAL TIMES RELATIVE TO MUSIC (t/t_{MUSIC}) FOR 8800 SIMULATION RUNS PER RANGE CELL (A TOTAL OF 52800 RUNS FOR EACH ARRAY TYPE).

VIII. CONCLUSION

Simulations of oceanographic HF radars using surface currents from ROMS provide a complex and demanding test of DOA methods. This analysis suggests improved performance from MLE-AP and WSF compared to MUSIC for the SeaSonde and RA-8 arrays, in that these DOA methods return more solutions than MUSIC when signals arrive from two or more bearings ($N > 1$) and SNR < 20 dB. The only substantial improvement in accuracy was found for the RA-8 when $N = 2$ and SNR< 20 dB – other accuracy results were mixed or the differences minor, e.g. a $1^o - 2^o$ advantage for MLE-AP with the ULA-16 when $N = 2$, or a 1^o advantage for MUSIC with the RA-8 and $N = 3$. Improvements come at higher computational cost, a factor of $8 - 15$ for MLE-AP over MUSIC. Overall the W-MUSIC and SML DOA methods exhibit inferior performance, though the further exploration of different weighting schemes for W-MUSIC may be worthwhile. If we use SNR as an inverse proxy for range, these results suggest that the use of MLE-AP (or WSF) would result in improved coverage in distant range cells for radars using SeaSonde and RA-8 arrays, and an improved ability to identify current structures presenting

the radar with $N \geq 2$. The ULA-16 produces very low σ_{RMS}, and the array has the potential to resolve more than the maximum of $N = 4$ signal sources used here, even with a narrower azimuthal view. Further investigations are required to thoroughly explore this capability.

Since DOA methods essentially work in conjunction with detection methods, further work is needed to translate these results to operational systems. Present detection methods in use (in particular for the SeaSonde [33]) work closely with the MUSIC algorithm, using ratios of the eigenvalues, and reconstructed signal powers, to determine the number of signal sources. Thus these methods are not appropriate for use with other DOA methods, since MUSICs limitations result directly from the use of the eigen-decomposition. It is possible that the empirical detection used here may perform better than algorithmic detection methods, such that the improved data returns observed for MLE-AP and WSF would be lost with "imperfect" detection. However, this analysis demonstrates the potential benefits of using MLE-AP and WSF given a suitable detection method. The similar performance found for WSF compared with MLE-AP may be useful, despite the significant computational demands, if its method for detection proves successful.

Investigations varying empirical signal detection suggest that the differences in performance between DOA methods are not sensitive to the specific designations of N used (shown in Fig. 2). In general, changing the boundaries of the regions affected the results of the different DOA methods more or less equally, e.g. shifting all the curves upward, without changing relative performance. The blank regions between different values of N in Fig. 2, were needed to minimize the impact of signal that was spread to adjacent Doppler bins (i.e. to adjacent velocities) by the FFT. In Fig. 2a for example, DOA methods would place solutions for $5 < \mathbf{v}_r < 10$ cm s^{-1} near 300^o, correctly identifying signal at that bearing that was spread from the adjacent Doppler bin (i.e. from the bin near 5 cm s^{-1}). In the σ_{RMS} calculation, large bearing errors would result, along with elevated σ_{RMS}. Future simulation runs could use longer FFT lengths to negate the need for the blank regions used in Fig. 2.

The discrete source analysis (section VII-A) illustrates the influence of source separation ($\Delta\theta$) on DOA performance. As $\Delta\theta \rightarrow 0.5\Delta\theta_{HPBW}$ (where $\Delta\theta_{HPBW}$ is the array half power beamwidth) MUSIC performance degrades, either in terms of DOA accuracy, or in terms of the number of solutions returned. Thus the relative magnitudes of $\Delta\theta_{HPBW}$ (a characteristic of the array) and $\Delta\theta$ (a characteristic of the flow field) have implications for oceanographic radars. For example, the large $\Delta\theta_{HPBW}$ of the SeaSonde dictates that a large $\Delta\theta$ is required for MUSIC

to resolve two signal sources. The performance advantage for MLE-AP with the SeaSonde – in the number of DOA solutions found in simulations with ROMS – results from the fact that $\Delta\theta$ presented by the ROMS surface currents are often less than $0.5\Delta\theta_{HPBW}$. Similarly the smaller $\Delta\theta_{HPBW}$ of the RA-8 results in a breakdown-like effect when $N = 2$ for MUSIC. ROMS flows present source $\Delta\theta$ that fall into the region where MUSIC breaks down and MLE-AP produces high accuracy. Meanwhile, $\Delta\theta_{HPBW}$ for the ULA-16 is sufficient to distinguish signal sources as presented by ROMS, using any of the DOA methods.

For the SeaSonde, radar simulations with ROMS often result in more simultaneous signal sources (spatial patches of ocean surface with similar radial velocity) than there are antennas ($N \geq M$). This is due in part to the spatial complexity of the ROMS currents. However, the frequency of $N \geq M$ also results from the assumption that each ROMS grid scatters equally, as if Bragg waves occur equally in all directions. Previous simulations (e.g. as modelled by [26]–[28]) assumed a primary wind direction, causing a preferred scattering direction. Adding wind to the simulation narrows the angular region of a range cell with relatively higher SNR. Narrowing the angular region has the effect of reducing N, by decreasing SNR at the off-wind bearings, such that they are close to noise. Simulations here result in $N \geq 2$ in about 78% of the time, compared with publish values of $< 50\%$ [33] from observations made with MUSIC. If the ocean presents radars with $N = 1$ a high fraction of the time, then the difference in ocean current maps produced with MUSIC or MLE-AP (or WSF) may not be significant. However, if $N \geq 2$ frequently occurs, then the differences with MLE-AP and WSF could be significant. Thus the overall significance of these results may depend on the angular distribution of N presented by real ocean environment.

This work has identified a potential for improvements in ocean current data produced by oceanographic HF radars, and reveals the need to identify and evaluate detection methods to use with MLE-AP and WSF. Further simulation based evaluations of detection methods are in progress, to be followed by the performance analysis of combined detection and DOA estimation methods applied to oceanographic HF radar observations.

ACKNOWLEDGMENT

Discussions with L. Washburn, A. Kirincich and C. Johnson significantly improved this effort. Simulation software was derived from software provided by Dr. D. Barrick, C. Whelan, and B.

Rector of Codar Ocean Sensors Ltd. L. Romero generously provided the ROMS fields. The UCSB Center for Scientific Computing provided computing resources: an NSF MRSEC (DMR-1720256) and NSF CNS-1725797. This material is based in part upon work supported by the National Science Foundation under Grant Number OCE-1658475. Any opinions, findings, and conclusions or recommendations expressed in this material are those of the author and do not necessarily reflect the views of the National Science Foundation.

REFERENCES

[1] I. Ziskind and M. Wax, "Maximum Likelihood Localization of Multiple Sources by Alternating Projection," *IEEE Transactions on Acoustics, Speech, and Signal Processing*, vol. 36, no. 10, pp. 1553–1560, 1988.

[2] J. Harlan, A. Allen, E. Howlett, E. Terrill, S. Y. Kim, M. Otero, S. Glenn, H. Roarty, J. Kohut, J. O'Donnell *et al.*, "National IOOS high frequency radar search and rescue project," in *OCEANS'11 MTS/IEEE Kona*. IEEE, 2011, pp. 1–9.

[3] A. R. Kirincich, T. De Paolo, and E. Terrill, "Improving HF radar estimates of surface currents using signal quality metrics, with application to the MVCO high-resolution radar system," *Journal of Atmospheric and Oceanic Technology*, vol. 29, no. 9, pp. 1377–1390, 2012.

[4] A. Kirincich, "The occurrence, drivers, and implications of submesoscale eddies on the Marthas Vineyard inner shelf," *Journal of Physical Oceanography*, vol. 46, no. 9, pp. 2645–2662, 2016.

[5] ——, personal communication.

[6] L. Romero, D. A. Siegel, J. C. McWilliams, Y. Uchiyama, and C. Jones, "Characterizing storm water dispersion and dilution from small coastal streams," *Journal of Geophysical Research: Oceans*, vol. 121, no. 6, pp. 3926–3943, 2016.

[7] A. F. Shchepetkin and J. C. McWilliams, "The regional oceanic modeling system (ROMS): A split-explicit, free-surface, topography-following-coordinate oceanic model," *Ocean Modelling*, vol. 9, no. 4, pp. 347–404, 2005.

[8] P. M. Kosro, "On the spatial structure of coastal circulation off Newport, Oregon during spring and summer 2001 in a region of varying shelf width," *Journal of Geophysical Research C: Oceans*, vol. 110, no. 10, pp. 1–16, 2005.

[9] R. Castelao, S. Glenn, O. Schofield, R. Chant, J. Wilkin, and J. Kohut, "Seasonal evolution of hydrographic fields in the central Middle Atlantic Bight from glider observations," *Geophysical Research Letters*, vol. 35, no. 3, pp. 6–11, 2008.

[10] P. R. Oke, J. S. Allen, R. N. Miller, G. D. Egbert, and P. M. Kosro, "Assimilation of surface velocity data into a primitive equation coastal ocean model," *Journal of Geophysical Research*, vol. 107, no. C9, pp. 1–25, 2002.

[11] J. O'Donnell, D. Ullman, M. Spaulding, E. Howlett, T. Fake, P. Hall, T. Isaji, C. Edwards, E. Anderson, T. McClay, J. Kohut, A. Allen, S. Lester, C. Turner, and M. Lewandowski, "Integration of Coastal Ocean Dynamics Application Radar (CODAR) and Short-Term Predictive System (STPS) Surface Current Estimates into the Search and Rescue Optimal Planning System (SAROPS)," National Technical Information Service, Springfield, VA 22161, Washington, DC 20593-0001, Tech. Rep., 2005.

[12] B. M. Emery and L. Washburn, "Uncertainty Estimates for SeaSonde HF Radar Ocean Current Observations," *Journal of Atmospheric and Oceanic Technology*, vol. 36, no. 2, pp. 231–247, 2019. [Online]. Available: https://doi.org/10.1175/JTECH-D-18-0104.1

[13] R. O. Schmidt, "Multiple Emitter Location and Signal Parameter Estimation," in *Proc. RADC Spectrum Estimation Workshop*, Griffiths AFB, Rome, New York, 1979, pp. 243–258.

[14] G. Bienvenu and L. Kopp, "Adaptivity to background noise spatial coherence for high resolution passive methods," *ICASSP '80. IEEE International Conference on Acoustics, Speech, and Signal Processing*, vol. 5, no. 1, pp. 307–310, 1980.

[15] R. O. Schmidt, "A signal subspace approach to multiple emitter location and spectral estimation," *PhD thesis, Stanford University, California. Schmidt, R*, vol. 34, no. 3, pp. 276–280, 1981.

[16] R. Schmidt, "Multiple emitter location and signal parameter estimation," *IEEE Transactions on Antennas and Propagation*, vol. 34, no. 3, pp. 276–280, 1986.

[17] B. J. Lipa and D. E. Barrick, "Least-squares methods for the extraction of surface currents from CODAR crossed-loop data: Application at ARSLOE," *IEEE J. Oceanic Eng.*, vol. 8, pp. 226–253, 1983.

[18] P. Broche, Y. Barbin, D. J. Maistre, P. Forget, and J. Gaggelli, "Antennas processing and design for VHF COSMER coastal radar," in *ROW-4 Radiowave Oceanography Workshop*, Townsville, Australia, April 21-23, 2004.

[19] Y. Barbin, P. Broche, J. de Maistre, P. Forget, and J. Gaggelli, "Practical results of Direction Finding method applied on a 4 antenna linear array WERA," in *ROW-6 Radiowave Oceanography Workshop, May 15-18.*, Hamburg, Germany, 2006.

[20] P. Forget, Y. Barbin, and G. Andre, "Monitoring of Surface Ocean Circulation in the Gulf of Lions (North-West Mediterranean Sea) Using WERA HF Radars," *IGARSS 2008 - 2008 IEEE International Geoscience and Remote Sensing Symposium*, pp. I–375–I378, 2008.

[21] A. Sentchev, P. Forget, Y. Barbin, and M. Yaremchuk, "Surface circulation in the Iroise Sea (W. Brittany) from high resolution HF radar mapping," *Journal of Marine Systems*, vol. 109-110, no. SUPPL., pp. 153–168, 2013.

[22] W. Wang and E. W. Gill, "Evaluation of beamforming and direction finding for a phased array hf ocean current radar," *Journal of Atmospheric and Oceanic Technology*, vol. 33, no. 12, pp. 2599–2613, 2016.

[23] D. E. Barrick and B. J. Lipa, "Radar angle determination with music direction finding," Nov. 23 1999, U.S. Patent 5,990,834.

[24] H. Krim and M. Viberg, "Two decades of array signal processing research: the parametric approach," *IEEE Signal Processing Magazine*, vol. 13, pp. 67–94, 1996.

[25] H. L. Van Trees, *Optimum array processing: Part IV of detection, estimation and modulation theory*. Wiley Online Library, 2002, vol. Part IV.

[26] D. E. Barrick and B. J. Lipa, "Comparison of direction-finding and beam-forming in HF radar ocean surface current mapping," *Phase 1 SBIR Final Report, Contract 50-DKNA-5-00092. National Oceanic and Atmospheric Administration, Rockville, MD.*, p. 81, 1996.

[27] K. E. Laws, D. M. Fernandez, and J. D. Paduan, "Simulation-based evaluations of HF radar ocean current algorithms," *IEEE Journal of Oceanic Engineering*, vol. 25, no. 4, pp. 481–491, 2000.

[28] T. de Paolo and E. Terrill, "Skill assessment of resolving ocean surface current structure using compact-antenna-style HF radar and the MUSIC direction-finding algorithm," *Journal of Atmospheric and Oceanic Technology*, vol. 24, no. 7, pp. 1277–1300, 2007.

[29] K. Laws, J. D. Paduan, and J. Vesecky, "Estimation and assessment of errors related to antenna pattern distortion in CODAR SeaSonde high-frequency radar ocean current measurements," *Journal of Atmospheric and Oceanic Technology*, vol. 27, no. 6, pp. 1029–1043, 2010.

[30] R. Chapman, L. Shay, H. Graber, J. Edson, A. Karachintsev, C. Trump, and D. Ross, "On the accuracy of HF radar surface current measurements: Intercomparisons with ship-based sensors," *Journal of Geophysical Research*, vol. 102, no. C8, p. 18737, 1997. [Online]. Available: http://doi.wiley.com/10.1029/97JC00049

[31] R. D. Chapman and H. C. Graber, "Validation of HF radar measurements," *Oceanography*, vol. 10, no. 2, pp. 76–79, 1997.

[32] H. C. Graber, B. K. Haus, R. D. Chapman, and L. K. Shay, "HF radar comparisons with moored estimates of current speed and direction: Expected differences and implications," *Journal of Geophysical Research*, vol. 102, no. C8, p. 18749, 1997.

[33] B. Lipa, B. Nyden, D. S. Ullman, and E. Terrill, "SeaSonde radial velocities: Derivation and internal consistency," *IEEE Journal of Oceanic Engineering*, vol. 31, no. 4, pp. 850–861, 2006.

[34] D. D. Crombie, "Doppler spectrum of sea echo at 13.56 Mc./s." *Nature*, pp. 681–682, 1955.

[35] D. E. Barrick, "First-order theory and analysis of MF-HF-VHF scatter from the sea," *IEEE Transactions on antennas and propagation*, vol. AP-20, no. 1, pp. 2–10, 1972.

[36] R. H. Stewart and J. W. Joy, "HF radio measurements of ocean surface currents," *Deep Sea Research*, vol. 21, pp. 1039–1049, 1974.

[37] E.-C. Ha, "Remote sensing of ocean surface current and current shear by hf backscatter radar," Stanford Electronics Lab, Stanford University, Tech. Rep. SU-SEL-79-022, 1979.

[38] C. C. Teague, J. F. Vesecky, D. M. Fernandez, and L. P. Atkinson, "HF radar instruments, past to present," *Oceanography*, vol. 10, no. 0704, pp. 40–44, 1997.

[39] J. Martinez-Pedraja, L. K. Shay, B. K. Haus, and C. Whelan, "Interoperability of seasondes and wellen radars in mapping radial surface currents," *Journal of Atmospheric and Oceanic Technology*, vol. 30, no. 11, pp. 2662–2675, 2013.

[40] T. de Paolo, T. Cook, and E. Terrill, "Properties of hf radar compact antenna arrays and their effect on the music algorithm," in *OCEANS 2007*. IEEE, 2007, pp. 1–10.

[41] P. Forget, "Noise properties of HF radar measurement of ocean surface currents," *Radio Science*, vol. 50, no. 8, pp. 764–777, 2015.

[42] A. R. Kirincich, "Improved detection of the first-order region for direction-finding HF radars using image processing techniques," *Journal of Atmospheric and Oceanic Technology*, vol. 34, no. 8, pp. 1679–1691, 2017.

[43] P. Stoica and R. L. Moses, *Spectral analysis of signals*. Upper Saddle River, NJ: Pearson Prentice Hall, 2005.

[44] B. Friedlander, "Wireless Direction-Finding Fundamentals," in *Classical and Modern Direction-of-Arrival Estimation*, T. E. Tuncer and B. Friedlander, Eds. Elsevier, 2009, ch. 1, pp. 1–49.

[45] M. Wax and T. Kailath, "Detection of signals by information theoretic criteria," *Acoustics, Speech and Signal Processing*, vol. 33, no. 2, pp. 387–392, 1985.

[46] *SeaSonde Radial Site Release 7 LLUV 1.12 File Format*, Codar Ocean Sensors, Ltd. [Online]. Available: http://support.codar.com/Technicians_Information_Page_for_SeaSondes/Docs/GuidesToFileFormats/File_LonLatUV_RDL_TOT_ELP.pdf

[47] S. Y. Kim, E. J. Terrill, B. D. Cornuelle, AA, S. Y. Kim, E. J. Terrill, and B. D. Cornuelle, "Mapping surface currents from HF radar radial velocity measurements using optimal interpolation," *Journal of Geophysical Research: Oceans*, vol. 113, no. 10, pp. 1–16, 2008. [Online]. Available: http://doi.wiley.com/10.1029/2007JC004244

[48] J. Kohut, H. Roarty, E. Randall-Goodwin, S. Glenn, and C. S. Lichtenwalner, "Evaluation of two algorithms for a network of coastal HF radars in the Mid-Atlantic Bight," *Ocean Dynamics*, vol. 62, no. 6, pp. 953–968, 2012.

[49] D. M. Kaplan and F. Lekien, "Spatial interpolation and filtering of surface current data based on open-boundary modal analysis," *Journal of Geophysical Research: Oceans*, vol. 112, no. 12, pp. 1–20, 2007.

[50] M. Yaremchuk and A. Sentchev, "Mapping radar-derived sea surface currents with a variational method," *Continental Shelf Research*, vol. 29, no. 14, pp. 1711–1722, 2009.

[51] P. Stoica and A. Nehorai, "Music, Maximum Likelihood, And Cramer-Rao Bound," *IEEE Transactions on Acoustics, Speech, and Signal Processing*, vol. 37, no. 5, pp. 720–741, 1989.

[52] M. Buijsman, Y. Uchiyama, J. McWilliams, and C. Hill-Lindsay, "Modeling semidiurnal internal tide variability in the southern california bight," *Journal of Physical Oceanography*, vol. 42, no. 1, pp. 62–77, 2012.

[53] Y. Uchiyama, E. Y. Idica, J. C. McWilliams, and K. D. Stolzenbach, "Wastewater effluent dispersal in southern california bays," *Continental Shelf Research*, vol. 76, pp. 36–52, 2014.

[54] W. C. Skamarock, J. B. Klemp, J. Dudhia, D. O. Gill, D. M. Barker, W. Wang, and J. G. Powers, "A description of the advanced research WRF version 2," National Center For Atmospheric Research Boulder Co Mesoscale and Microscale Meteorology Div, Tech. Rep., 2005.

[55] D. E. Barrick and J. B. Snider, "The Statistics of HF Sea-Echo Doppler Spectra," *IEEE Journal of Oceanic Engineering*, vol. 2, no. 1, pp. 19–28, 1977.

[56] E. Tuncer and B. Friedlander, *Classical and modern direction-of-arrival estimation*. Academic Press, 2009.

[57] P. Stoica and A. Nehorai, "Performance Study of Conditional and Unconditional Direction-of-Arrival Estimation," *IEEE Transactions on Acoustics, Speech, and Signal Processing*, vol. 38, no. 10, pp. 1783–1795, 1990.

[58] M. Viberg, B. Ottersten, T. Kailath, and M. V. Ottersten, "Detection and estimation in sensor arrays using weighted subspace fitting," *IEEE Transactions on Signal Processing*, vol. 39, no. I, pp. 2436–2449, 1991.

[59] P. Stoica and K. C. Sharman, "Maximum likelihood methods for direction-of-arrival estimation," *Acoustics, Speech and Signal Processing, IEEE Transactions on*, vol. 38, no. 7, pp. 1132–1143, 1990.

[60] D. E. Barrick and B. J. Lipa, "Evolution of bearing determination in hf current mapping radars," *Oceanography*, vol. 10, no. 2, pp. 72–75, 1997.

[61] P. Flament, D. Harris, M. Flament, I. Fernandez, L. Benjamin, P. Milne, J. McClean, L. Mari, I. Rodriguez, J. Bencomo, and X. Flores, "Design and implementation of a compact low-power controller for hf doppler radars," 2017, radiowave Oceanography Workshop, Lüneburg, Germany, 19-21 Sept. 2017.

[62] B. M. Emery, L. Washburn, C. Whelan, D. Barrick, and J. Harlan, "Measuring antenna patterns for ocean surface current hf radars with ships of opportunity," *Journal of Atmospheric and Oceanic Technology*, vol. 31, no. 7, pp. 1564–1582, 2014.

[63] B. A. Johnson, Y. I. Abramovich, and X. Mestre, "MUSIC, G-MUSIC, and maximum-likelihood performance breakdown," *IEEE Transactions on Signal Processing*, vol. 56, no. 8, pp. 3944–3958, 2008.

[64] Y. I. Abramovich, B. A. Johnson, and X. Mestre, "DOA Estimation in the Small-Sample Threshold Region," in *Classical and Modern Direction-of-Arrival Estimation*, T. E. Tuncer and B. Friedlander, Eds. Academic Press, 2009, ch. 7, pp. 219–287.